Mohamed Khider University of Biskra
Faculty of exact sciences and natural and life sciences
Material sciences department

MASTER MEMORY

Domain of Matter Sciences
Section of Physics
Speciality of Energy Physics and Renewable Energies

Réf. :

Prsentedd by:
Khadraoui Yousra

The :

Dependence of Zinc Oxide (ZnO) Thin Films Properties Elaborated By SILAR on the Number of Cycles

---

Jury:

Mrs.	Ben Naceur Kheira	MCB	University Med Khidar of Biskra	President
Mr.	Rahmane Saâd	Pr	University Med Khidar of Biskra	Supervisor
Mrs.	Hamani Nadjette	MCB	University Med Khidar of Biskra	Examiner

Academic Year: 2022\2023

Acknowledgements

Before all, I thank **Allah** who gave me all the courage and the will to go till the end for the accomplishment of this work.

I express my deep gratitude and sincere appreciation to my teachers and supervisors

Pr. Saâd RAHMANE

for the time he devoted to me and for his follow-up during the period of realization of my project.

My thanks are also extended to the members of the jury for reviewing my work.

My thanks and appreciation go to many people in the Laboratory of Thin Films at Mohamed Khider University who, from near or far, have contributed to the achievement of this work.

Finally, thanks go to all my teachers at the Material Sciences Department of Biskra.

Dedication

I dedicate this work to my dear parents, my father **Said** and my mother **Nabila** for their endless advice, encouragement, and support as a testimony of my gratitude, in the hope that they will be proud.

To my dear brother **Dr.Mohamed Amine**.

To my nephew **Mohamed Mehdi**.

To my lovely sisters **Sara**, **Soumaya**, **Amani**, **Sabrine**, and **Meriem Sirine**.

To my friends **Chaima** and **Manar**.

To all my family and friends.

To all my dear ones.

Contents

List of Figures

List of Tables

General Introduction

After the success of integrated circuits in electronics, significant efforts have been made to develop optical circuits based on thin films in order to overcome the problems generally encountered in conventional optics. The field of integrated optics is currently the subject of intense and very promising research, particularly in the field of telecommunications and signal processing (amplifiers, micro-lasers, multiplexers, etc.).

Minimizing these losses is the primary objective of most optical materials studies. To remedy this, we remain convinced that the understanding of their origins and their consequences on the properties of the waveguide are necessary for a reassessment of their method of elaboration [1].

In recent years, transparent conductive oxides (TCO) have been the subject of numerous research works. The development of these materials is linked to their interesting physical properties which combine electrical conduction and optical transparency in the visible spectral range. In particular, zinc oxide, this material a serious candidate for various applications [2].

A deposition technique is considered the integral key for the creation of new materials thin film to meet the ever-increasing demand from industries for versatile and multi-dynamics materials. The deposition techniques determine virtually all the properties of the thin film and can also be used to modify the existing properties. Proper consideration needs to be given to the deposition techniques depending on the area of application because not all deposition techniques result in identical properties such as microstructure, surface morphology, tribological, electrical, biocompatibility, optical, corrosion, and hardness.

In addition, a combination of different techniques can be used to form a hybrid deposition process with each contributing to the outcome of the thin film [3].

The objective of our work is : Optimization of the quality of ZnO thin films by studying

the influence of the number of SILAR cycles on thin film properties.

In addition to a general introduction to the subject, our research work is presented in a report structured into three chapters as follows:

- **CHAPTER 1: BIBLIOGRAPHIC RESEARCH**

  The first chapter brings together the results of bibliographical research on the transparent conductive oxide (TCO) "definition, properties, applications ..." and particularly the Zinc oxide "properties, areas of application...".

- **CHAPTER 2: THIN FILM DEPOSITION TECHNIQUES AND CHARACTERIZATION METHODS**

  The second chapter is devoted to the description of the techniques for producing thin films such as CVD (chemical vapor deposition), Spray pyrolysis, and Sol-Gel, as well as the methods for characterizing the thin films used in this work, UV-Vis spectroscopy, X-Rays Diffraction (DRX) and the Four-point method as well as Atomic Force Microscopy (AFM).

- **CHAPTER 3: EXPERIMENTAL PART AND DISCUSSION**

  In this chapter, we give special attention to the deposition technique of thin films by the Successive Ionic Layer Adsorption and Reaction **"SILAR"**.

  This chapter also exposes the various experimental results obtained (structural, optical, morphological, and electric properties) from thin films of ZnO elaborated by the SILAR technique with a discussion and comparison of these results.

Finally, we finish this report with a general conclusion in which we identify all the significant results that we have obtained during this work and some perspectives for research in the more or less long term.

Bibliography

[1] B Benrabah. *Etude des Propriétés Physico-chimiques des Couches de SnO2 Préparées par la Technique «dip-coating*. PhD thesis, Université Mohamed Boudiaf Oran, 2010.

[2] S Rahmane. *ELABORATION ET CARACTERISATION DE COUCHES MINCES PAR SPRAY PYROLYSE ET PULVERISATION MAGNETRON*. PhD thesis, Université Mohamed Khider Biskra, 2008.

[3] O O Abegunde, E T Akinlabi, O Ph Oladijo, S Akinlabi, and A U Ude. Overview of thin film deposition techniques. *AIMS Materials Science*, 6(2):174–199, 2019.

Chapter I

Bibliographic Research

I.1 Introduction

The first chapter will tackle bibliographic research. It's devoted to the definition of Semiconductors, Transparent conductive oxide (TCO), and Zinc Oxide (ZnO), in addition to then some properties (crystallographic, electrical, optical, etc.) and Zinc oxide applications.

I.2 Semiconductor

According to energy band theory, three electrical states are possible: metal, insulator, and semiconductor.

In metal, the conduction band (CB) and valence band (VB) overlap, allowing the free flow of electrons. The semiconductor, meanwhile, has a forbidden band that separates VB and CB commonly called gap, and denoted Eg. Electrons cannot take energies located in this band. They must acquire energy to cross CB. For a higher gap, we speak of insulation because even at room temperature, CB is empty. Their difference is more than 4 eV [1].

I.2.1 Definition of Semiconductor

The semiconductor is usually defined rather loosely as a material with electrical resistivity lying in the range of $10^{-2} - 10^{9}(\Omega.cm)$ [2]. In general, the main factors that determine the basic properties (e.g., optical and electrical properties) of semiconductors are related to the chemical composition and the (crystallographic) structure, the presence of various defects

and impurities (both intentional and unintentional), and the dimensions of the semiconductor or semiconductor structure. The chemical composition and the (crystallographic) structure determine the electronic band structure (e.g., the magnitude and the type of energy gap, and the carrier effective mass), which has the major influence on the semiconductor properties. The electrical conductivity of semiconductors can be varied widely as a function of [3] :

- Impurity content (doping).
- Temperature (thermal excitation).
- Optical excitation (excitation with photons having energies greater than the energy gap Eg).
- Excess charge carrier injection.

In the doping of semiconductor material, extra levels of impurities are added. In n-type materials, the electron energy levels are near the top of the band gap It causes easy excitation into the conduction band. In the case of P-type materials extra holes in the band gap allow the excitation of valance band electrons. Mobile holes are left in the valance Band [4], as shown in Figure I.1 [5].

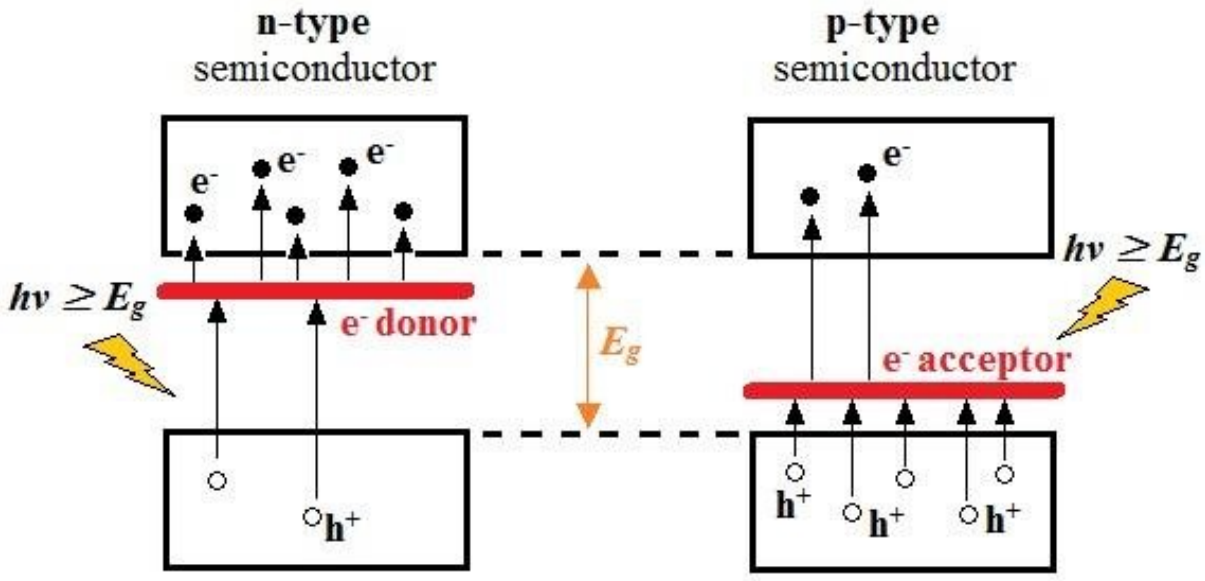

Figure I.1: Illustration of n and p-type doping in a semiconductor.

I.2.2 Types of Semiconductors

- **Elemental Semiconductors**

  The important elemental semiconductors are group IV materials, such as silicon (Si), germanium (Ge), and diamond (C). These group IV elemental materials all have a diamond crystal structure, each atom is in a tetrahedral configuration with the four nearest atoms, and thus they are also referred to as tetrahedrally-bonded semiconductors [3].

- **Compound Semiconductors**

  - **II–VI Compounds**, The Zn and Cd-chalcogenides (i.e., compounds with O, S, Se, and Te) cover a wide range of electronic and optical properties due to the wide variations in their energy gap, Since all the II–VI compound semiconductors have direct energy gaps, efficient emission or absorption of electromagnetic radiation can be expected [3].
  - **III–V Compounds** formed from elements of group III and V of the periodic table have properties very similar to their group IV counterparts [2]. Many of these compounds (e.g., GaAs, InAs, InP, and InSb) have direct energy gaps and high carrier mobilities thus, the common applications of these semiconductors are in a variety of optoelectronic devices for both the detection and generation of electromagnetic radiation and also in high-speed electronic devices. The energy gap of these compounds, which are useful for optoelectronic applications [3].
  - **IV–VI Compounds** The lead chalcogenides (i.e., PbS, PbSe, and PbTe) are characterized by narrow energy gaps, high carrier mobilities, and high dielectric constants. The unique feature of the direct energy gap in these compounds increases with increasing temperature [3].

- **Oxide Semiconductors**

  Although most oxides are good insulators, some such as ZnO, SnO_2, and Cu_2O are well-known semiconductors in general, in addition, they are polycrystalline and polyphase materials, the properties of the grains and grain boundaries play a crucial role in both the understanding and applications of these materials. In this context, the control of the

composition and microstructure, especially, grain boundaries are the most important issues in developing these materials [2, 3].

- **Other Types of Semiconductors** [2, 3]
  - **Organic Semiconductors**.
  - **Magnetic Semiconductors**.
  - **Amorphous Semiconductors**.

I.3 Transparent conductive oxide (TCO)

I.3.1 Definition of TCO

In general, TCO thin film is a material that has a resistivity in the order of $10^{-3}(\Omega.cm)$ or less, and an average transmittance above 80% in the visible range and band-gap energy above approximately 3 eV.

I.3.2 Properties of TCO

I.3.2.1 Optical Properties

The optical properties depend on the interaction of the electromagnetic wave with the electrons of the material [6], where the Optical transmission is defined as the ratio between the intensity of incident light and the intensity of light transmitted through the material under consideration [1]. The optical properties of materials are governed by three essential phenomena which are transmission, reflection, and absorption, these phenomena being characterized by the parameters T (Transmittance), R (reflection), A (absorption factor), and α (absorption coefficient). [7], the Beer-Lambert law makes it possible to relate these phenomena by the equation [1]:

$$T = (1 - R)\exp^{-\alpha.d} \tag{I.1}$$

T: the transmission coefficient.

R: the reflection coefficient.

d: the thickness of the film considered.

α: the absorption coefficient depending on the wavelength λ.

The transmission properties of TCO are defined by depending on the wavelength λ, as illustrated by figure I.2 :

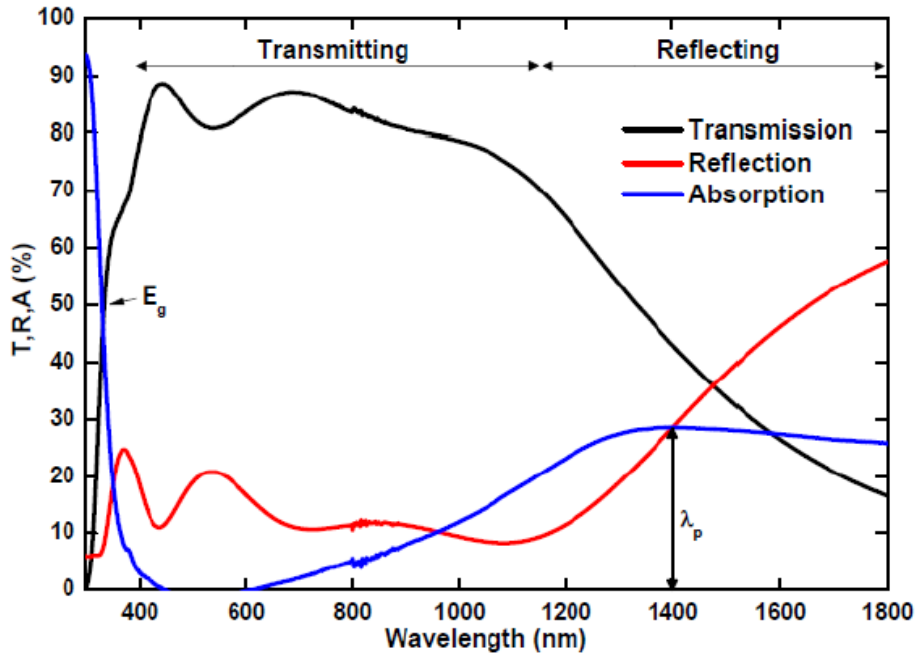

Figure I.2: Transmission, Reflection and absorption spectra of a typical TCO.

The existence of an optical window covering the entire visible range is characteristic of TCO, add to that we distinguishing in the figure I.2 three regions [8]:

- Strongly absorbing region in the short wavelength range due to bandgap excitation of the oxide.
- Transparent region in the visible.
- Reacting region due to free carriers past a characteristic wavelength in the infrared (IR).

In addition to λp, At this wavelength, the thin films absorbs part of the incident radiation. This absorption peak due to the presence of free electrons in the material depends on their concentration and their mobility.

The transmission in the visible may be attenuated slightly by absorption of un-reacted species in the oxide, or reaction by scattering at rough surfaces, however, it is usually above 80%.

I.3.2.2 Electrical Properties

- **Conduction due to Vacancies**

  A stoichiometric oxide is an insulator, so perfect stoichiometry does not exist in TCOs. Indeed, in the crystalline structure, certain oxygen atoms leave their site and pass into the surrounding gaseous phase, leaving behind them anion vacancies that trap the two electrons of the O^{-2} ion. This corresponds to the appearance of an energy level in the forbidden band, close to the conduction band. Fairly low energy will then make it possible to activate these trapped electrons which will pass into the conduction band, causing ionization of the vacancies.

  When the vacancy rate is high, the interaction between the vacancies can no longer be neglected and the extension of the corresponding energy levels leads to the formation of a continuous band associated with the vacancies which, by widening, will cover gradually the conduction band. The ionization energy of vacancies becomes zero. The oxide is in this case degenerate. The fermi level then passes into the conduction band [6].

- **Conduction due to impurities**

  Doping is another way to modify the conductivity of the oxide. To do this, during production, a certain number of atoms of the compound are replaced by foreign atoms. This, in electronic design, results in the appearance of intermediate levels in the bandgap. The difference between the boundary of the conduction band and the donor level introduced is called the activation energy of the impurity and is equivalent to its ionization energy.

  The increase in the number of impurities has the effect of the appearance of a continuous band. When the concentration of impurities increases beyond a certain critical concentration, this band forms a coalescence with the conduction band and the activation energy becomes zero, the semiconductor behaves like a metal. He is said to be degenerate [6].

I.3.3 Criteria for Choosing TCO

TCO must have high electrical conductivity and low visible absorption. the figure of merit and denoted Φ_{TC} expressed in Ω^{-1} is the relationship between the transmission coefficient T and the surface resistance R_S, according to the relation. This figure of merit allows a comparison between different TCOs [1].

$$\Phi_{TC} = \frac{T^{10}}{Rs} \tag{I.2}$$

Alongside the electrical and optical properties, other criteria influence the choice of materials and its deposition method. The diversity of TCOs and their applications corresponds to the fact that the criterion for choosing a TCO does not depend solely on the factor of deserved. Other parameters relating to the material, its toxicity, its etching properties and its production costs, must be taken into consideration. In the domain of thin films, the frequency of the plasma, the homogeneity of the deposit and its surface roughness, the stabilities thermal, chemical and mechanical, adhesion to the substrate, and heat treatments minimum requirements are also important [7].

I.4 Zinc Oxide (ZnO)

I.4.1 Zinc Oxide Properties

Since the end of the 1990s, zinc oxide has attracted a great deal of interest, as evidenced by the surge in the number of publications related to this material [9]. Zinc oxide is a material belonging to the family of transparent conductive oxides (TCO) [10]. It is an II–VI oxide semiconductor with the formula ZnO [11]. The non-toxicity and abundance on earth of this compound make it an ideal candidate in several areas. Zinc oxide can exist in nature as a powder or as a massive crystal, color varies according to the impurities it contains (its red color, for example, is due to the presence of manganese within the material; while pure, it is transparent/white) and according to its deviation from stoichiometry [10], It is insoluble in water but soluble in acids and alcohols, also having a melting temperature is greater than 2250 °K, density is 5675 Kg.m^{-3}, enthalpy of formation is 6.5×10^5 J.mol^{-1} and shear modulus is equal to 44 GPa [12].In addition, having a wide direct band gap value of 3.2 to 3.37 eV along

with a large excitation binding energy (B.E) of 60 meV at room temperature [13]. Practically, ZnO is n-type due to its native defects created during preparation due to excess zinc in the interstitial position or oxygen vacancy, or both [11].

I.4.1.1 Structural Properties

ZnO is a compound semiconductor with a tetrahedral bonding configuration, where each anion is surrounded by four cations at the corners of a tetrahedron, and vice versa, corresponding to the sp3 covalent bonding. However, ZnO exhibits large ionicity, which increases the bandgap beyond that expected from the covalent bonding [14]. Zinc oxide can crystallize in three forms: the Hexagonal Wurtzite structure, the Zinc-Blende structure, and the Cubic Rocksalt structure (NaCl) [6] as shown in figure I.3. None of the three crystal structures of

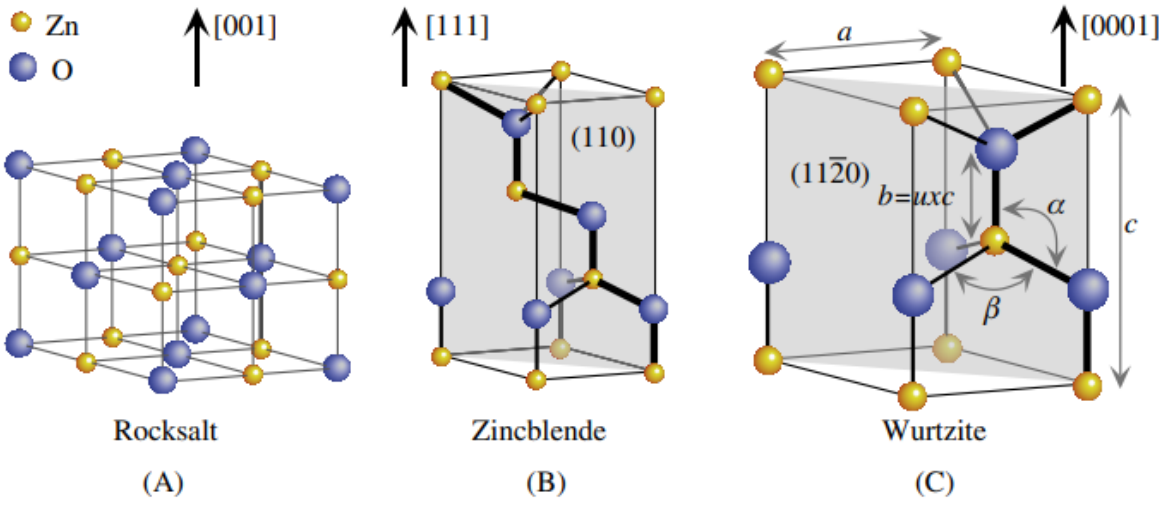

Figure I.3: Stick and ball representation of ZnO crystal structures: (A) Cubic Rocksalt, (B) Cubic Zinc-Blende, and (C) Hexagonal Wurtzite.

ZnO possesses inversion symmetry; therefore, the ZnO crystal exhibits crystallographic polarity, which indicates the direction of the bonds [14]. ZnO in a Zinc-Blende structure can only be stable if the film growth is on cubic substrates, Rocksalt structure can be synthesized under high pressure (above 10 Gpa at room temperature). Under ambient conditions, Hexagonal Wurzite is the most thermodynamically stable structure [6]. The easiest way to see the unit cell is to look at the tetrahedron shown in Figure I.4 [15].

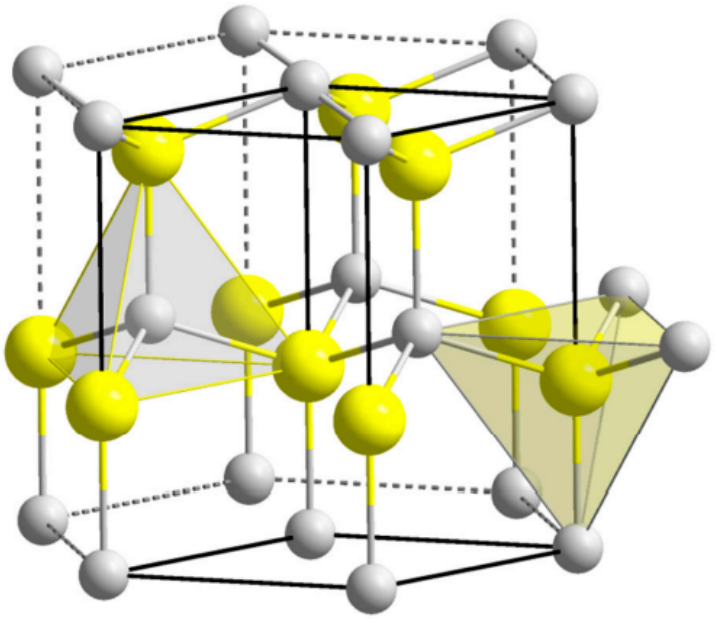

Figure I.4: ZnO wurtzite cell, Zn in yellow, O in grey.

This structure is a stack of compact double layers (Zn and O), along the [0001] axis, also called the c axis. In this Wurtzite structure, the lattice parameters of ZnO are: a = 0,32495 nm, c = 0,52069 nm. The hexagonal lattice of the Wurtzite structure consists of an interpenetration of sublattices of the O^{-2} anion and the Zn^{+2} cation, each of which is composed of four atoms of the same type [12]. the wurtzite structure deviates from the ideal arrangement by changing the $\left(\frac{c}{a}\right)$ ratio [14].

I.4.1.2 Electrical Properties

The electronic structure of the zinc and oxygen [11] is:

$$O : 1s^2 2s^2 2p^4$$

$$Zn : 1s^2 2s^2 2p^6 3s^2 3p^6 3d^1 04s^2$$

In Fig I.5, the electronic density of the state associated with the direction reveals that the valence band is formed by the linear combination of the atomic orbitals of the 2p electrons of oxygen while the conduction band is generated by that of the atomic orbitals 4s electrons from zinc [16], it gives the value of 3,21 eV for the band gap of ZnO, i.e. a value in relatively good agreement with other authors, as stated in [10] the forbidden band can vary between 3,16 and 3,39 eV.

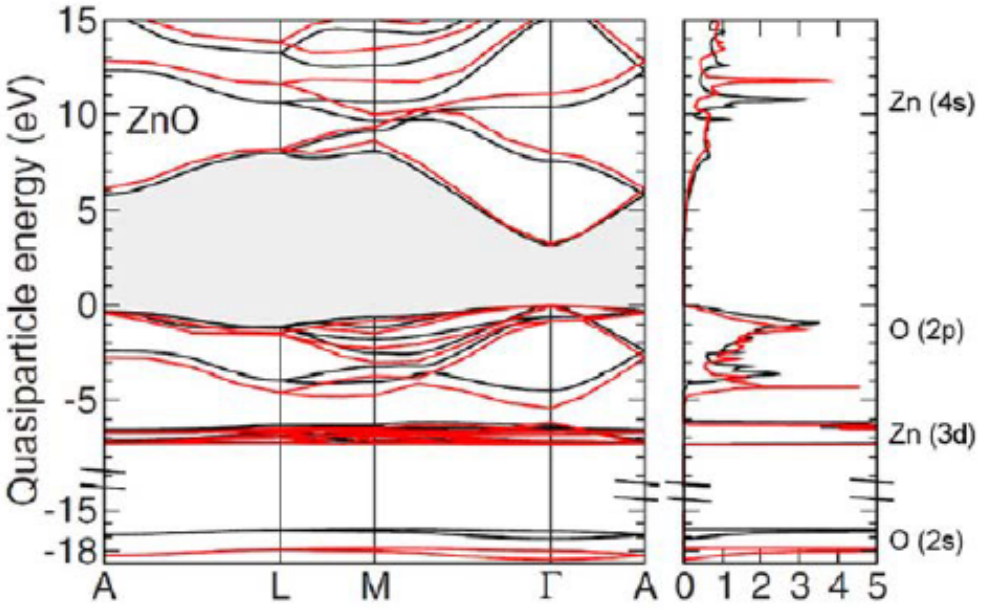

Figure I.5: Band diagram (left) and density of states (right) of ZnO.

ZnO has a direct band gap, which allows it to be classified among the wide band gap semiconductors. Depending on the method of preparation and the doping rate, the bandgap value and by consisting the electrical properties can be modified widely. Two structural defects can create permitted bands in the forbidden band and ensure electrical conduction within the material:

- Either by deviating from stoichiometry, mainly by the introduction of excess zinc atoms in the interstitial position (Zn_i) or by the creation of anionic oxygen vacancies (Vo).
- Or by cationic substitution, by substituting zinc or oxygen atoms with foreign atoms of different valence where we obtain p-type and n-type ZnO [6].

The main cause of p-type doping difficulty is due to the compensation of the dopants by the native defects existing in the material such as (Zn_i and Vo) [6] where very low formation energies for oxygen vacancies and zinc interstitials in ZnO have likely to explain the native n-type conductivity observed in as-grown films [11].

I.4.1.3 Optical Properties

In the form of a thin film, the optical properties of ZnO depend on the preparation conditions, the heat treatment applied, film thickness, the deposition method used, the type and concentration of the dopant, and the type of substrate used. For example, improving the stoichiometry of zinc oxide leads to an increase in the optical gap and a decrease in the absorption coefficient. in addition, in the case of better crystal quality, it is likely to pass visible light up to 90%. The refractive index has a value that varies between 1,90 and 2,20 depending on the authors [6, 10], with values of band gap between 3,16 and 3,39 eV.

I.4.2 Applications of ZnO

- **ZnO Powders**

  ZnO provides better color retention, greater covering power, greater durability, and protection against ultraviolet rays, due to its ability to absorb these rays, which is why it is much used in the paint industry. The rubber industry is the biggest consumer of zinc oxide, with 57% of the market. A quantity of 20 to 30% added, improves the thermal conductivity, the wear resistance, and slows down the aging of the rubber. It also enters the ceramics industry, participating in the manufacture of glass, porcelain, and sinters, because it makes it possible to reduce the coefficient of expansion and improve tensile stability. It can also be used for the manufacture of varistors because, in the presence of small quantities of metal oxides, zinc oxide has excellent properties of electrical non-linearity. This allows it to be widely used in the protection of electronic devices and in particular in high-voltage stations [6].

- **ZnO Thin Films**

  - **Photovoltaic**

    In principle, a solar cell is a system made up of semiconductor materials that consist of transforming solar energy into direct current [10]. The heterojunction between two types of p-n semiconductors generates the formation of an induced current under the photons of light. A depletion zone forms at the contact between the n-type semiconductor (ZnO) and the p-type one, accompanied by the creation

of an electric field. Electrons and holes will recombine at the level of the depletion zone. Placed under illumination, the charges will be separated by the energy of the photons and by the electric field which will induce the formation of a current (Figure I.6 (a)) [17].

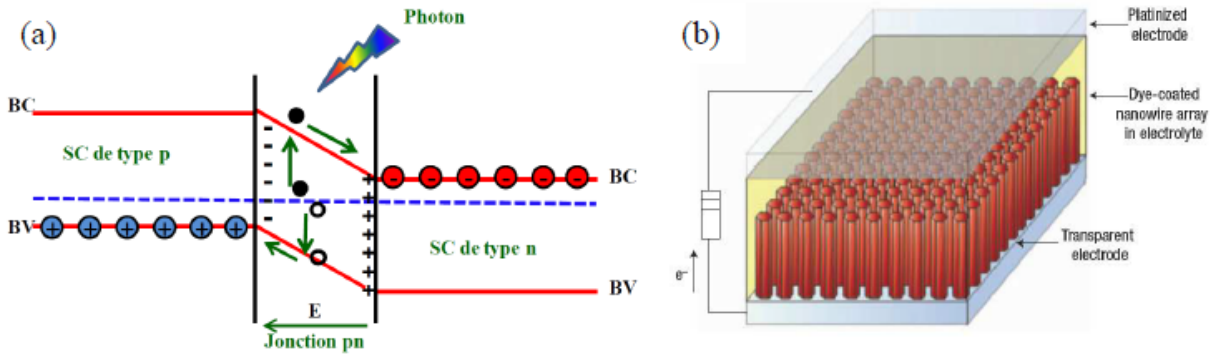

Figure I.6: Principle of charge separation under illumination (a) and cell photovoltaic based on ZnO nanowires (b).

The 3^{rd} generation dye-sensitized solar cells (DSSC) have been studied in Another possibility is to work on the anode, consisting of a metal oxide (TiO_2, SnO_2, ZnO), it was synthesized in the form of films whose thickness exceeded the diffusion length of the electron limiting the performance of the cell. The development of anodes based on nanostructures of metal oxides has improved the properties of electronic diffusion and charge collection. Because of an increase in the specific surface, a greater quantity of dye can be adsorbed on the surface, thus increasing the electronic transfer rate. Nanostructures with controlled dimensions make it possible to optimize the transport of charges between the dye, the metal oxide anode, and the transparent electrode by reducing the diffusion distances (Figure I.6 (b))[17].

– **Piezoelectric Sensor**

The piezoelectric effect in ZnO thin films is related to its non-centrosymmetric crystallographic structure, which causes deformation upon application of external forces. This is due to the appearance of an electric potential difference between

the surfaces of the film. In addition, the application of an external electric field to the material causes a displacement of the ions of the elementary meshes, by electrostatic forces, which generates the mechanical deformation of the crystal. Due to their piezoelectric properties, thin films of ZnO are good candidates for the fabrication of various electronic devices (rectifiers, filters, resonators for radio communications, and image processing devices).In addition, it is used as a surface acoustic wave device [9]. The acoustic wave is generated on the surface of the ZnO film due to the application of the potential difference to the electrodes [10].

– **Photocatalytic**

With industrial development, environmental pollution exacerbates and yields high amounts of organic contaminants, and this phenomenon is a serious environmental problem. The use of solar power with semiconductor-based heterogeneous photocatalysts has been extensively investigated and the potential applications of sunlight have been presented to remove organic contaminants and noxious bacteria. The efficiency of photocatalysts, such as ZnO is generally determined by light absorption [18].

The photodegradation of pollutants by using ZnO is illustrated in Fig I.7. Photocatalysis occurs as the ZnO photocatalyst is irradiated by light with energy larger than its bandgap energy [18, 19], where excite electrons (e^-) from the valence band to the conduction band and holes (h^+) are produced in the valence band. The photogenerated valence band holes react with either water (H_2O) or hydroxyl ions (OH^-) adsorbed on the catalyst surface to generate hydroxyl radicals (•OH) which are strong oxidants. The photogenerated electrons in the conduction band may react with oxygen to form superoxide ions ($•O_2^-$).

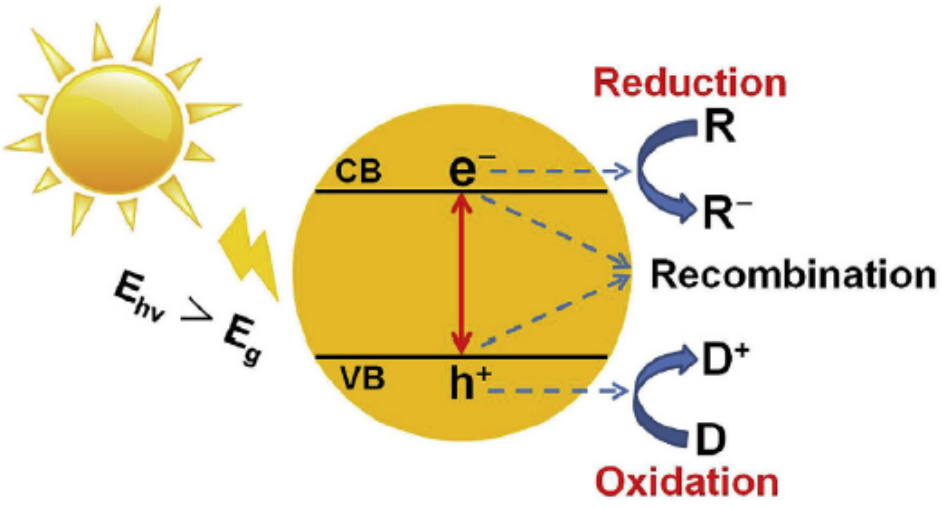

Figure I.7: The basic mechanism of ZnO photocatalysis.

Consequently, H_2O molecules can be oxidized by these holes to form hydroxyl radicals. These highly reactive radical groups (•OH, O_2^-• directly oxidize organic pollutant molecules in solutions [18].

– **Gas Sensor**

Zinc oxide is a wide-gap semiconductor whose conductivity strongly depends on the nature of the surrounding gas. Thus, the presence of a reducing gas (CO, H_2, etc.) will lead to an increase in the electrical conductivity of ZnO thin films, while the presence of an oxidizing gas will result in the opposite behavior. Indeed the performance of a gas sensor (Sensitivity, Selectivity, Stability, Reversibility, Coverage, and repeatability) is closely linked to the materials used, whether in terms of their composition, morphology, or their surface condition. Due to its chemical properties, zinc oxide becomes a good candidate for gas detection. Gas sensors based on zinc oxide have been used for the detection of nitrogen dioxide or carbon monoxide. Other aluminum-doped ZnO-based gas sensors have very high sensitivity and excellent selectivity for amino gases such as dimethylamine and triethylamine [10].

Bibliography

[1] J Garnier. *Elaboration de couches minces d'oxydes transparents et conducteurs par spray cvd assiste par radiation infrarouge pour applications photovoltaïques*. PhD thesis, Arts et Métiers ParisTech, 2009.

[2] M Cardona and Y Y Peter. *Fundamentals of semiconductors*, volume 619. Springer, 2005.

[3] B G Yacobi. *Semiconductor materials: an introduction to basic principles*. Springer Science & Business Media, 2003.

[4] Y Singh. *Semiconductor devices*. IK International Pvt Ltd, 2013.

[5] O Monfort and G Plesch. Bismuth vanadate-based semiconductor photocatalysts: a short critical review on the efficiency and the mechanism of photodegradation of organic pollutants. *Environmental Science and Pollution Research*, 25:19362–19379, 2018.

[6] S Rahmane. *ELABORATION ET CARACTERISATION DE COUCHES MINCES PAR SPRAY PYROLYSE ET PULVERISATION MAGNETRON*. PhD thesis, Université Mohamed Khider Biskra, 2008.

[7] A Allag. *Optimisation des conditions d'élaboration des couches minces d'oxyde d'étain SnO2 par spray*. PhD thesis, Université Mohamed Khider–Biskra, 2018.

[8] A A Assi and W R Saleh. Conductive polymer dye sensitive solar cell (dssc) for improving the efficiency. *PhD diss., Ph. D. Thesis, University of Baghdad*, 2014.

[9] T Pauportè. Synthesis of zno nanostructures for solar cells—a focus on dye-sensitized and perovskite solar cells. In *The Future of Semiconductor Oxides in Next-Generation Solar Cells*, pages 3–43. Elsevier, 2018.

[10] S Boulmelh. Élaboration et caractérisation d'un dépôt de couches minces d'oxyde de zinc par spray pyrolyse. *mémoire de magister, univ. Frères Mentouri Constantine*, 2015.

[11] M Dahnoun. *Preparation and characterization of Titanium dioxide and Zinc oxide thin films via Sol-Gel (spin coating) technique for optoelectronicapplications*. PhD thesis, University Mohamed Khider Biskra, 2020.

[12] N Kouidri. *Contribution à l'étude de couches minces d'oxydes transparents conducteurs à base de zinc et cobalt par spray pneumatique*. PhD thesis, University of Mohamed Khider, BISKRA, 2019.

[13] P Chaudhary and V Kumar. Preparation of zno thin film using sol-gel dip-coating technique and their characterization for optoelectronic applications. *World Scientific News*, (121):59–66, 2019.

[14] Ü Özgür, V Avrutin, and H Morkoç. Zinc oxide materials and devices grown by molecular beam epitaxy. In *Molecular Beam Epitaxy*, pages 343–375. Elsevier, 2018.

[15] M A Borysiewicz. Zno as a functional material, a review. *Crystals*, 9(10):505, 2019.

[16] S Guillemin. *Mécanismes de croissance de nanostructures de ZnO par voie chimie liquide et caractérisation avancée*. PhD thesis, INSA de Lyon, 2014.

[17] C Ch César. *Élaboration et caractérisation de capteurs de gaz à base de nanofils de ZnO*. PhD thesis, Université Paris-Est, 2013.

[18] K Qi, B Cheng, J Yu, and W Ho. Review on the improvement of the photocatalytic and antibacterial activities of zno. *Journal of Alloys and Compounds*, 727:792–820, 2017.

[19] E S Elmolla and M Chaudhuri. Degradation of amoxicillin, ampicillin and cloxacillin antibiotics in aqueous solution by the uv/zno photocatalytic process. *Journal of hazardous materials*, 173(1-3):445–449, 2010.

Chapter II

Thin Film Deposition Techniques and Characterization Methods

II.1 Introduction

This chapter consists of two parts. In the first part, we will present thin films deposition techniques according to the physical and chemical way, while in the second part, we will present characterization methods of the thin films such as X-ray diffraction (XRD), UV-VIS spectroscopy, Atomic Force Microscopy (AFM), and the four-point technique.

II.2 Deposition Techniques

A thin film is defined as a material created by the random nucleation and growth processes of individually condensing/reacting atomic/ionic/molecular species on solid support called a substrate. Thin films encompass a considerable thickness range, varying from a few nanometers to micrometers. Thin films have very interesting properties that are quite different from those of the bulk materials from which they are made of. As the film becomes thinner, the surface properties become more important than the bulk [1]. The physical properties of the thin film depend not only on its chemical composition but also on the method used for its preparation. Thin films are produced using a wide variety of techniques due to the diversity of applications for this material. They can be obtained by operating in the liquid phase or in the vapor phase and by physical or chemical processes [2]. The atomistic random nucleation

and growth processes give new exotic properties to thin film materials. These properties can be controlled and reproduced by precisely modulating a range of deposition parameters [1]. Figure II.1 shows techniques classification used for thin film deposition [3].

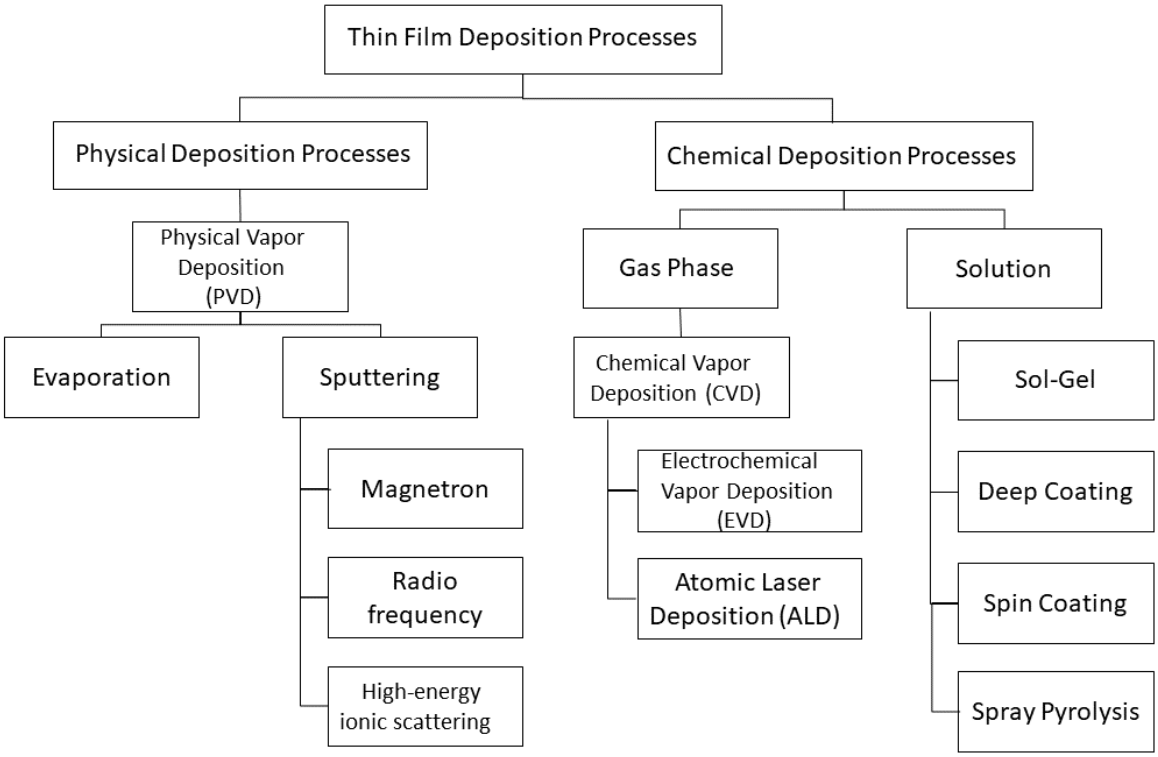

Figure II.1: Classification of thin film techniques.

II.2.1 Physical processes

II.2.1.1 Physical Vapor Deposition (PVD)

Physical vapor deposition can be divided into several categories: vacuum evaporation (a), sputter deposition in a plasma environment (b,c) and in a vacuum (d), ion planting in a plasma environment with a thermal evaporation source (e), with a sputtering source (f) and with an arc vaporization source (g) and ion-assisted deposition (IBAD) (h), as shown in Figure II.2. The most common physical vapor deposition processes are Sputtering and Evaporation [3]. All these techniques are based on the same principle, the process of which involves three fundamental steps [2]:

- the vaporization of the material to be deposited.

- the transport of these species in vapor phases from the source to the substrate.
- the condensation of these same species on the surface of the substrate and the growth of the film.

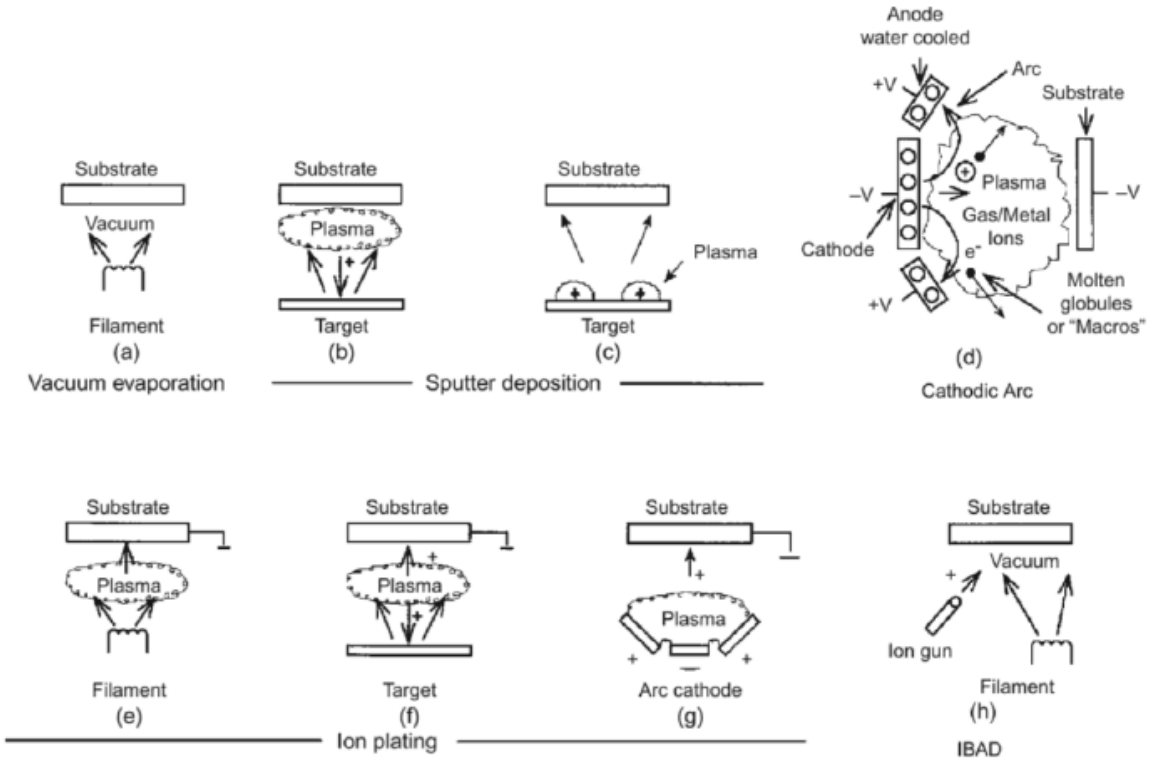

Figure II.2: Physical vapor deposition Processing Techniques.

– **Evaporation**

Evaporation, which is sometimes called vacuum deposition, is the simplest method of physical vapor deposition. This technique is conducted in a vacuum system, where the material is heated to temperatures close to its melting or sublimation point [3].

The main problems generally encountered during evaporation are [2]:

* The dissociation of oxides.
* The reaction of the materials to be evaporated with those with which they are in contact.
* Degassing, decomposition, and micro-explosions of the materials to be evaporated.

* The difficulty of obtaining layers of alloys having the same composition as the starting alloy.

– **Sputtering**

In a basic sputtering process, a target (or source) material, to be deposited onto a substrate, is bombarded by energetic ions, typically inert gas ions, such as Argon (Ar^+). The forceful collision of these inert gas ions onto the target cause the removal (known as sputtering) of target atoms, which condense on the substrate as a thin film of stoichiometry similar to that of the target material. Though the basic idea of the operation is apparently simple, the actual mechanisms involved in sputtering are quite complex. Nonetheless, the process is limited by low deposition rates, high substrate heating, and low ionization efficiencies [4]. Physical sputtering has a number of methods, for example: Radio Frequency (RF) magnetron sputtering, as well as high-energy ionic scattering. Radio frequency magnetron sputtering is an elective technique on account of its inherent versatility, low-temperature deposition, and uniform surface coverage. Fig II.3 shows a schematic of the reactive RF magnetron sputtering [5].

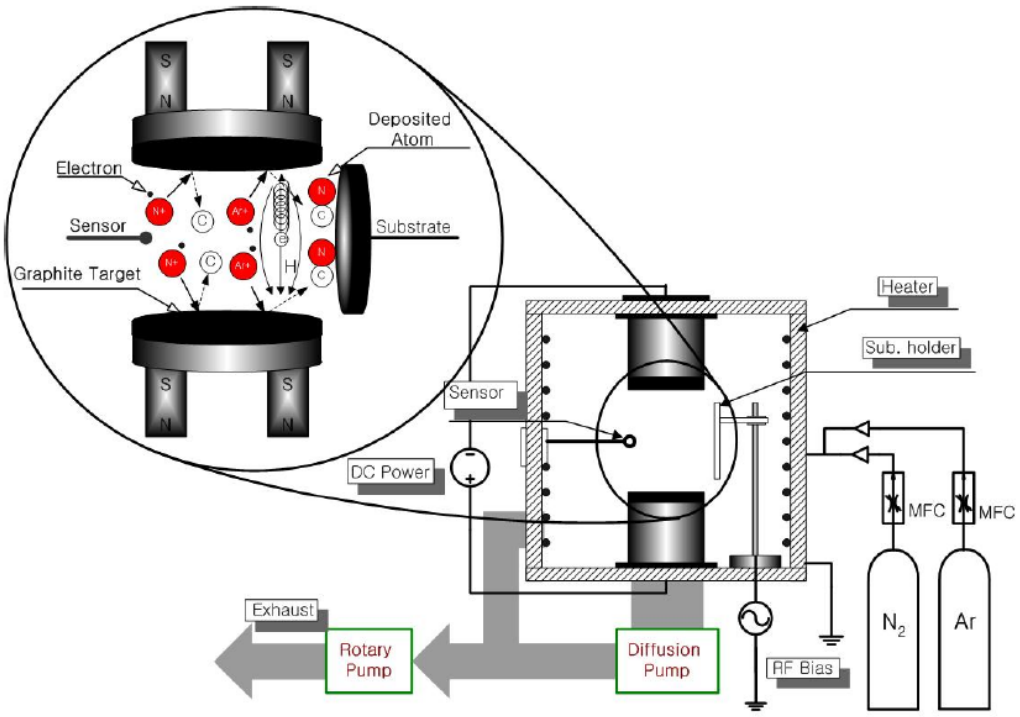

Figure II.3: A schematic diagram of facing target RF magnetron sputtering system.

The sputtering method removes surface atoms from a solid cathode by bombarding it with positive ions from an inert gas, for example, argon, discharges, and next deposits them on the surface to create a thin layer. Substrates are positioned in a vacuum chamber and are pumped down to a specified process pressure. If a negative charge occurs on the target material, sputtering starts. This causes plasma or glow discharge. Positively charged ions of gas created in the plasma area are attracted extremely quickly to the negatively biased target plate. This interaction causes a momentum transfer and ejects atomically sized particles from the target. Those particles are accumulated on the substrate surface as a thin layer [3].

II.2.2 Chemical Processes

II.2.2.1 Chemical Vapor Deposition (CVD)

The chemical vapor deposition (CVD) process is one in which a gaseous phase chemically reacts to produce one or more condensed phases (deposit) plus gaseous product species. A typical laboratory or industrial CVD process would involve a dynamic flow system in which gaseous reactants pass over a heated substrate. These gases react chemically to produce a condensed coating on the substrate plus product gases, and then these product gases plus any remaining reactant gases exit from the hot reaction zone. The CVD process can be described in terms of the system's chemistry (chemical species, thermodynamics, kinetics, reaction mechanisms), mass transport (gaseous diffusion, forced convection), and gaseous flow behavior (types of flow, flow patterns, velocities) [6]. Among the methods of synthesis we distinguish [2]:

- Plasma-Enhanced Chemical Vapor Deposition (PECVD).
- CVD at Atmospheric Pressure (AP-CVD).
- Low-Pressure CVD (LP-CVD).

A net CVD process can be described by a series of mechanistic steps, Fig II.4 shows these steps [6] :

1. Forced flow of reactant gases into the system.

2. Diffusion and flow of reactant gases through the gaseous boundary layer to the substrate.
3. Adsorption of gases onto the substrate.
4. Chemical reactions of the adsorbed species, or of adsorbed and gaseous species.
5. Desorption of adsorbed species from the substrate.
6. Diffusion and flow of product gases through the boundary layer to the bulk gas.
7. Forced exit of gases from the system.

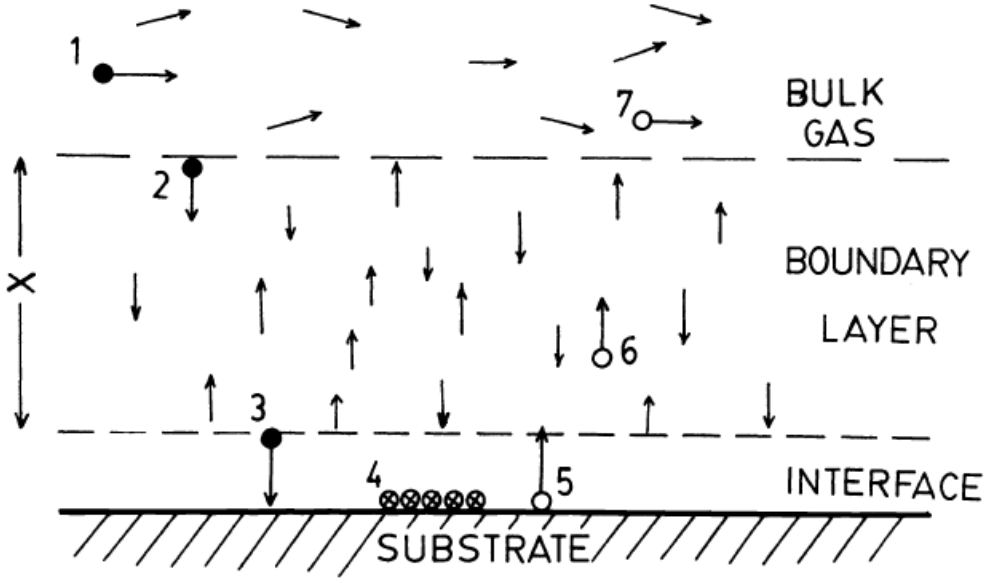

Figure II.4: Schematic Diagram Showing CVD Process.

These processes make it possible to obtain crystallized films without having to resort to annealing with very variable thicknesses on both insulating and conductive substrates, which also have excellent adhesion. The main weaknesses associated with these techniques are the deformation of the substrate due to the thermal gradient and the diffusion of impurities from the heated substrate [2].

II.2.2.2 Sol-Gel

The Sol-Gel process is a fairly recent technique for the synthesis of ceramic materials in the solid state in the form of thin layers for example. It consists of the hydrolysis and conden-

sation of chemical precursors [2]. The Sol–Gel process, called also soft chemistry ("chimie douce"), allows the elaboration of a solid material from a solution by using a sol or a gel as an intermediate step, and at much lower temperatures than is possible by traditional methods of preparation.

Fig II.5 shows the main steps of preparation of thin films and powder by Sol–Gel process [7].

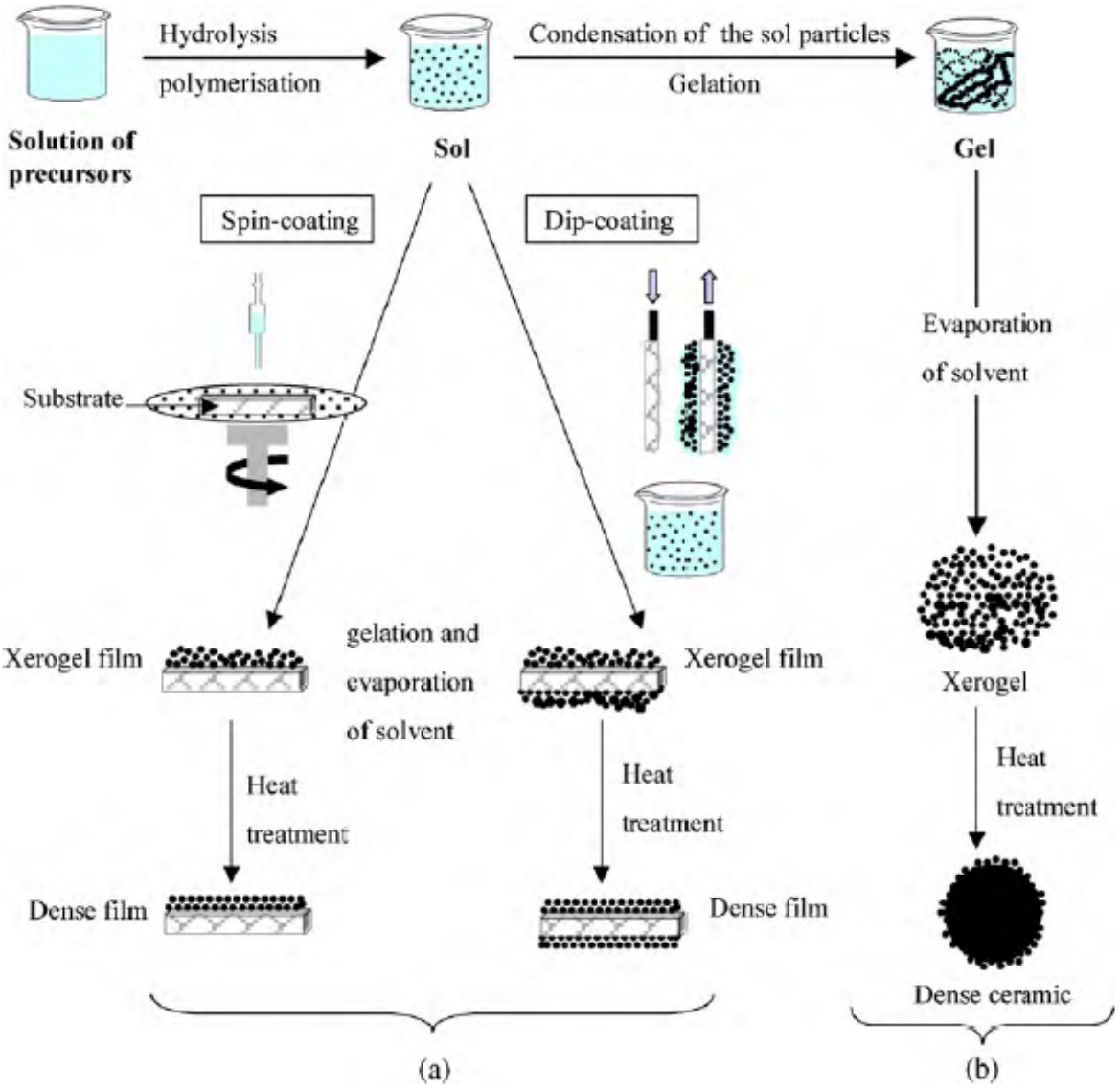

Figure II.5: Two synthesis examples by the sol-gel method; (a) Thin films ; (b) powder.

We can summarize the film preparation in three parts:

1. Preparation of the precursor solution.

2. Covering the substrate with a solution, the evaporation of the solvent causes the chemical species to come together which can then react with each other to form a film (xerogel)[2] by the chosen technique.

3. Heat treatment of the xerogel film.

In addition, thin film deposition involves several parameters: the nature of the precursor and its concentration, the type of solvent and the acidity of the medium, the type of additive species and their concentrations, the aging time of the early mixture, the method of coating of substrates and its speed, the nature of the substrate, and the pre-and post-heat treatment of the materials [7].

The most used techniques for Sol-Gel are "Spin-Coating" and "Dip-Coating" [2] where:

- **Dip-Coating**

  Dip coating designates the deposition of a wet liquid film by the withdrawal of a substrate from a liquid coating medium. The process of film formation in total implies several technical stages as demonstrated in Figure II.6 [8].

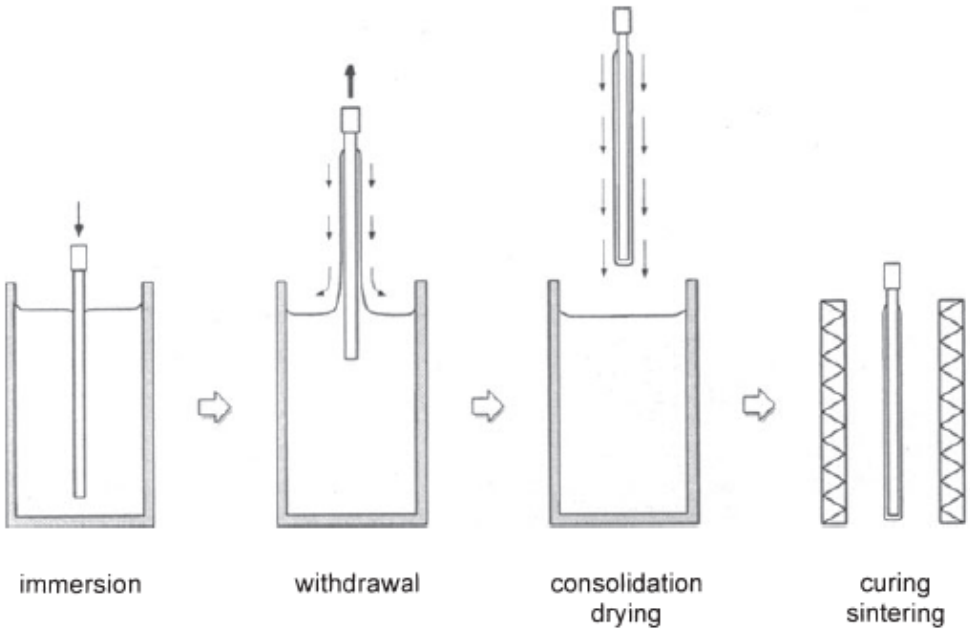

Figure II.6: Fundamental stages of sol-gel dip coating .

But nevertheless, the underlying chemical and physical processes are mostly overlapping. Starting with the immersion of the substrate, a coherent liquid film is entrained

on the withdrawal of the substrate from the coating fluid, which then consolidates by drying and accompanying chemical reactions. To obtain the final coating material, normally a further curing or sintering step (post-treatment) is then necessary [8].

- **Spin-Coating**

  The Spin-Coating method is a simple and quick thin film preparation method. It can offer ultrathin polymer film with even thickness [9]. Spin-coating consists of spreading the sol by centrifugation on a substrate rotating at a high speed. This process begins first by depositing an excess of soil on the stationary substrate, then the latter is rotated, for this purpose, the liquid is spread and the excess liquid deposited is evacuated. The continuous evaporation of the solvent and the polymerization of the deposit leads to a xerogel layer just like for the Dip-Coating [2] as shown in Fig II.7.

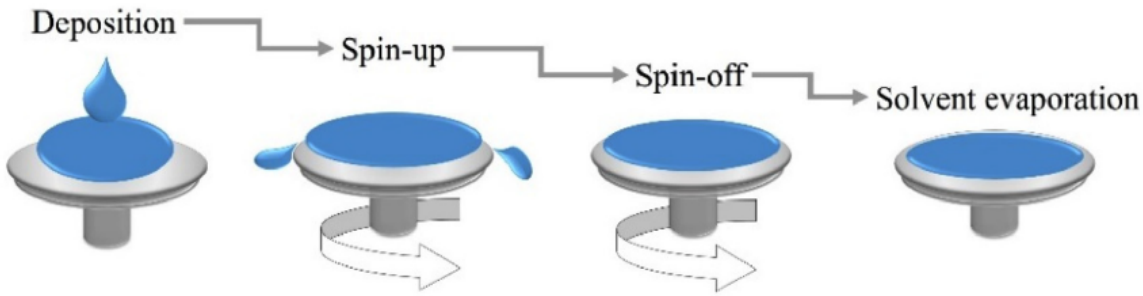

Figure II.7: Schematic diagram of thin film formation in Spin-Coating method.

The main drawback of this technique is the low deposition thickness which is around (50 nm) after one pass of the process. Thus, an iteration of the stages of spreading and evaporation of the solvent must be carried out in order to obtain a thickness of several hundred nanometers, which multiplies the risks of cracking because the first layers deposited undergo all the successive annealings of evaporation. control the crystallographic orientation [2].

II.2.2.3 Spray Pyrolysis

It consists of: **spray** and **pyrolysis**.

"Spray" is a word that indicates the jet of a liquid in fine droplets, launched by a sprayer [2].

"Pyrolysis" comes from pyrolytic and indicates the heating of the substrate. There is a thermal decomposition of a source to release a metal or a compound. The temperature of the substrate provides the necessary energy, called activation energy, to trigger the chemical reaction between the compounds [10].

The experiment can be carried out in air and can be prepared in an enclosure (or in a reaction chamber) under a vacuum of approximately 50 Torr [2]. Generally, the thickness of the layer deposited by this method depends on the concentration of the precursor, the volume of the solution to be sprayed, and the deposition time [11].

Fig II.8 shows The general simplified schema for spray pyrolysis deposition [12], where three steps can be viewed [2, 11]:

1. Generation of the aerosol: Droplets are generated by the atomizer at the outlet of the nozzle.

2. Transport of the aerosol: the transport of the species sprayed towards the substrate is carried out by a compressed gas (compressed air), electrostatic field.

3. Decomposition of the precursor to initiating film growth.

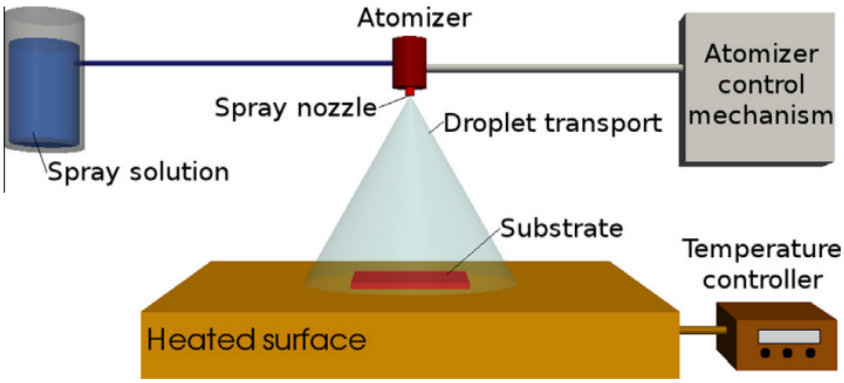

Figure II.8: General schematic of a spray pyrolysis deposition process.

II.3 Characterization Methods

After thin film production, it is necessary to carry out various characterizations, which make it possible to observe and optimize the influence of several factors of deposition such as temperature, concentration of doping, flow rate ... etc, that these layers will be analyzed by different characterization techniques.

The characterization of thin films is based on the following methods:

II.3.1 Thickness Measurements

The thickness of a film is a significant factor that affects the film's properties, for example, the dielectric constant, resistivity [13], and transmittance.

The film thickness can be determined by different methods such as: Gravimetric, Scanning Electron Microscopy, Swanepoel, and AFM Tip-Scratch.

The thickness d of our films is calculated using the gravimetric method by the following equation [10]:

$$d = \frac{m}{\rho \times A} \tag{II.1}$$

where :

m : is the mass of the deposited layer (g).

ρ **:** is the density (g/cm^3).

A : is the surface of the sample (cm^2).

II.3.2 Structural Characterization

X-ray diffraction is now a common technique for the study of crystal structures. This study is for the purpose of specifying the structure and crystallographic growth directions of the layers, to measure the lattice parameters and the size of the crystallites. It must also make it possible to examine the state of the stresses in the deposits.

II.3.2.1 X-Ray Diffraction

This method only applies to materials presenting the characteristics of the crystalline state, that is to say, an ordered and periodic arrangement of the atoms which constitute them [10].

These X-rays are generated by a cathode ray tube, filtered to produce monochromatic radiation, and directed toward the sample (with CuK_{α} radiation = 1.5418 °A) [14] at an angle θ (Figur II.9), and a detector receives the beam of X-rays diffracted by this sample and records its intensity as a function of the diffraction angle 2θ [2], The directions in which the interferences are constructive, called "diffraction peaks" (see Figur II.10), can be determined very simply by Bragg's formula law [10]:

$$2d_{hkl} \sin\theta = n\lambda \tag{II.2}$$

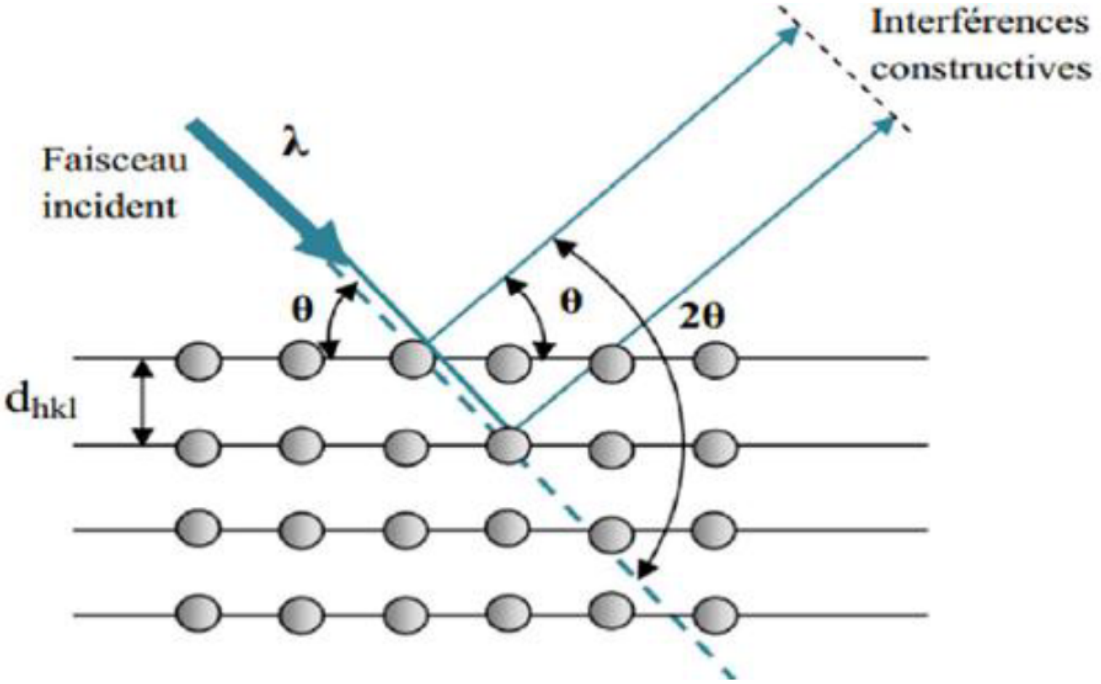

Figure II.9: Bragg diffraction diagram.

where:

d_{hkl} : Inter-reticular distance, ie distance separating the index planes (hkl).

θ **:** The angle of incidence of X-rays on the surface of the material studied.

n : Order of reflection (integer).

λ **:** X-ray wavelength.

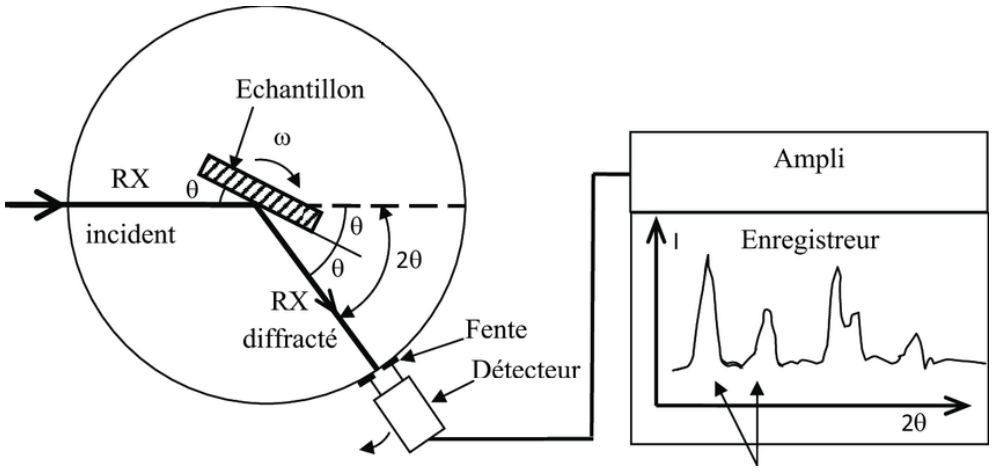

Figure II.10: Diagram of a diffractometer and X-ray diffraction spectrum.

II.3.2.2 Mesh Parameters Determination

By comparing our X-ray spectra with the JCPDS card (Joint Comity Powder Diffraction System) (Carte No: 36-1451) of Zinc oxide, we were able to identify the diffraction peaks, the (hkl), as well as the type of crystalline lattice. By using Bragg's law, we can determine the distances between reticular d_{hkl}. To calculate the lattice parameters (a and c), we take the most intense peak which corresponds to the preferential orientation of the hexagonal lattice of ZnO, and apply the relation II.3 [10]:

$$d_{hkl} = \frac{a}{\sqrt{\frac{4}{3}(h^2 + k^2 + hk) + l^2 \frac{a^2}{c^2}}} \tag{II.3}$$

where:

d_{hkl} : interreticular distance.

c, a : crystal parameter.

(hkl) : Miller indices.

The comparison of the value obtained for the parameters a and c with the theoretical values (a_0 = b_0 = 3,2498 °A, c_0 = 5,2066 °A of the JCPDS Card No.00-036-1451) gives information on the stress state in the considered film [15].

II.3.2.3 Crystallite Size Determination

By measuring the width of the peaks at half maxima (FWHM), it is possible to determine the average size of the crystallites. For this calculation, the Scherrer formula is used [16]:

$$D = \frac{k\lambda}{\beta \cos\theta} \tag{II.4}$$

where:

D: the average crystallite size (nm).

k: equals 0.9 (assuming the particles are spherical in shape).

λ **:** X-ray wavelength.

β **:** the FWHM.

θ **:** the angle of the measured diffraction peak (rad).

II.3.2.4 Strain Determination

Internal forces in the matter are known as stresses. When each crystallite is subjected to a different stress, neighboring peaks are juxtaposed, If the stress causes elastic deformation of the crystal lattice, this will change the interarticular distances d and shift the position of the peaks.

The strains "ε" can be calculated by the following formula [10]:

$$\varepsilon = \frac{\beta \cos\theta}{4} \tag{II.5}$$

II.3.3 Optical Characterization

In our study, we used UV-visible spectroscopy, by which we were able to measure curves representing the variation of the transmittance as a function of the wavelength. By exploiting these curves, it is possible to estimate the thickness of the film and to determine its optical characteristics; such as optical absorption edge, absorption coefficient, band gap width, and Urbach energy.

II.3.3.1 Transmittance Spectra

The transmission coefficient, or transmittance T, is defined as the ratio of the transmitted light intensity to the incident light intensity [15] according to the following equation [17]:

$$T = (1 - R)\exp^{-\alpha.d} \tag{II.6}$$

With α the absorption coefficient of the material.

If we consider a homogeneous material, of thickness d, at normal incidence, the quantity of light transmitted or transmittance T, expressed in % is defined by:

$$T = (\frac{I}{I_0}) \times 100 \tag{II.7}$$

where :

the light transmitted at the output is written according to the Beer-Lambert law [2]:

$$I = I_0 \exp^{-\alpha.d} \tag{II.8}$$

Figure II.11 shows the transmittance spectrum of ZnO thin film elaborated by SILAR method.

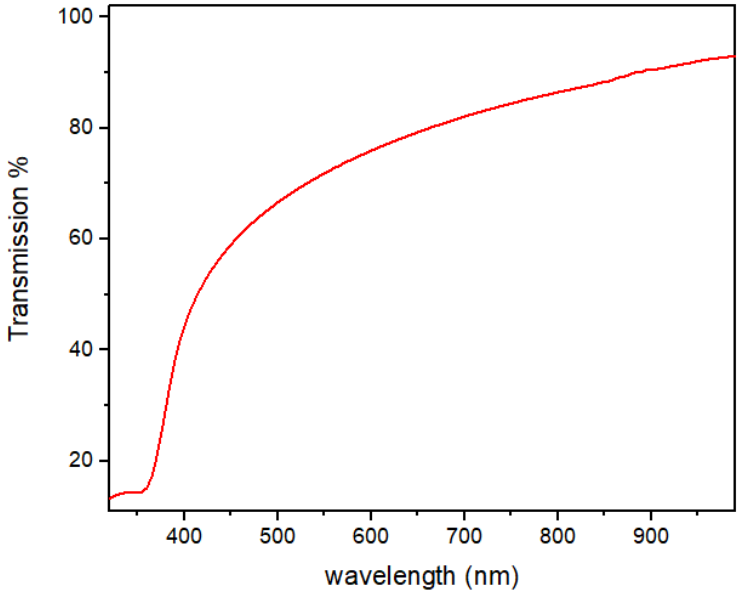

Figure II.11: The transmittance spectrum as a function of wavelength.

II.3.3.2 Optical Band Gap

In the high absorption domain, the gap value Eg corresponds to direct transitions within crystallized materials [15], this gap value can be deduced from the transmission spectrum by applying Tauc model [18]:

$$(\alpha h\nu)^n = A[h\nu - Eg] \tag{II.9}$$

where: Eg is the optical gap energy.

A: is a constant

and n = 2 or $\frac{1}{2}$ following a direct or indirect gap transition. Then, for a direct gap such as that of ZnO, α is expressed as a function Eg according to the following equation:

$$(\alpha h\nu)^2 = A[h\nu - Eg] \tag{II.10}$$

The method consists initially in calculating the absorption coefficient α in cm^{-1} according to the following equation [2]:

$$\alpha = (\frac{1}{d}) \ln (\frac{1}{T}) \tag{II.11}$$

Where:

d: is the thickness.

T: the transmittance.

For a direct transition semiconductor, the method then consists in plotting the curve $(\alpha h\nu)^2 = f(h\nu)$ where $h\nu$ is the photon energy in eV. The extrapolation of the linear part of the curve with the abscissa axis (Energies) gives the value of Eg (i.e. $(\alpha h\nu)^2 = 0$) [10], as shown in Figure II.12.

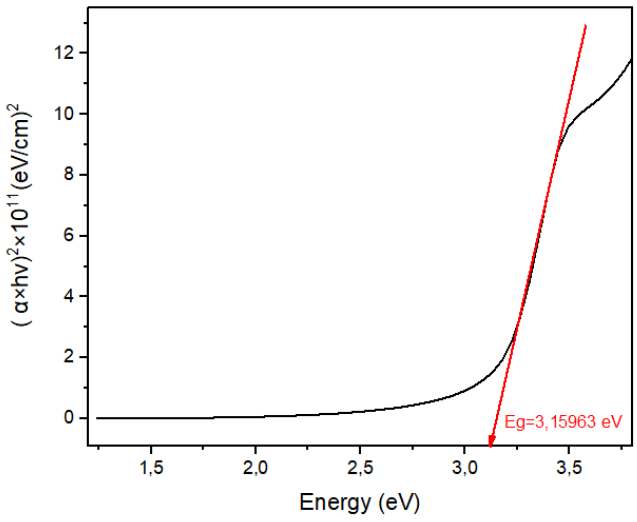

Figure II.12: Gap energy determination.

II.3.3.3 Urbach Energy

When in a material there are variations in interatomic distances, bond lengths, or angles, what is called "disorder" occurs. In this case, the band edges described in the case of crystal lattices and delimited by Ev and Ec can disappear. We observe what is called localized states formed in band tails at the boundaries of the forbidden band in the valence and conduction bands. For energies greater than Ec and less than Ev, there are extended states [15], This variation results in “blurring” of the valence-conduction bands and narrows slightly the band gap [19] as shown in Fig II.13.

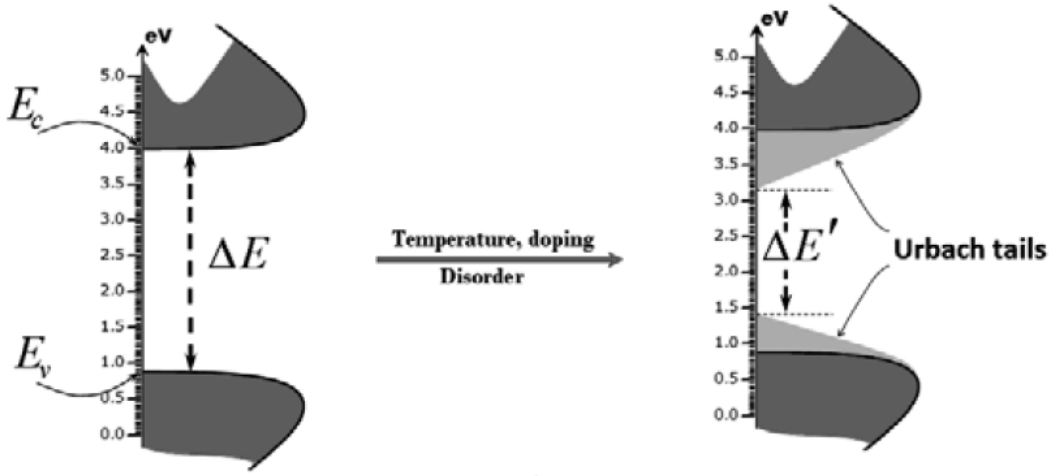

Figure II.13: Urbach tailing schema.

In 1953, Urbach identified unexpected exponential tails at the edges of optical interband in some impure crystals, resulting in short hybrid excitonic transitions. Electronic hopping occurs exceptionally between these localized states. According to the Urbach-Martienssen model, Urbach energy Eu represents the main parameter that determines the phonon capture efficiency of a semiconductor layer. It is defined through the equation II.12 [19]:

$$\alpha(h\nu) = \alpha_0 \exp^{\frac{h\nu}{Eu}} \tag{II.12}$$

where :

α is the absorption coefficient and α_0 is a constant.

By plotting $\ln(\alpha)$ as a function of $h\nu$ (FigII.14), we can access the determination of Eu value [15] :

$$\ln(\alpha) = \ln(\alpha_0) + \frac{h\nu}{Eu} \tag{II.13}$$

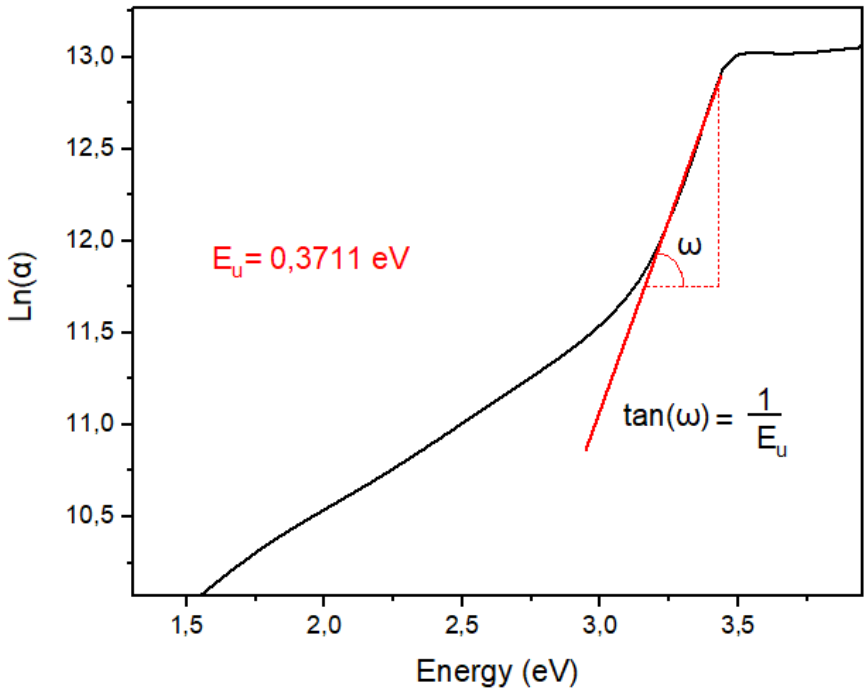

Figure II.14: Urbach energy determination.

II.3.4 Morphological Characterization

This characterization makes it possible to visualize the surface of the layers. In our study, we used Atomic Force Microscopy (AFM).

II.3.4.1 Atomic Force Microscopy (AFM)

The typical configuration of an AFM is shown in Fig II.15. The operation principle of the AFM is very similar to that of a stylus profilometer:

A sharp cantilever tip interacts with the sample surface, sensing the local forces between the molecules of the tip and the sample surface, it is the most sensitive part of an AFM. This instrument is not a conventional microscope that collects and focuses light. The word microscope has been associated with this instrument because it is able to measure the microscopic

features of the sample. The most characteristic property of the AFM is that the images are acquired by "feeling" the sample surface without using light.

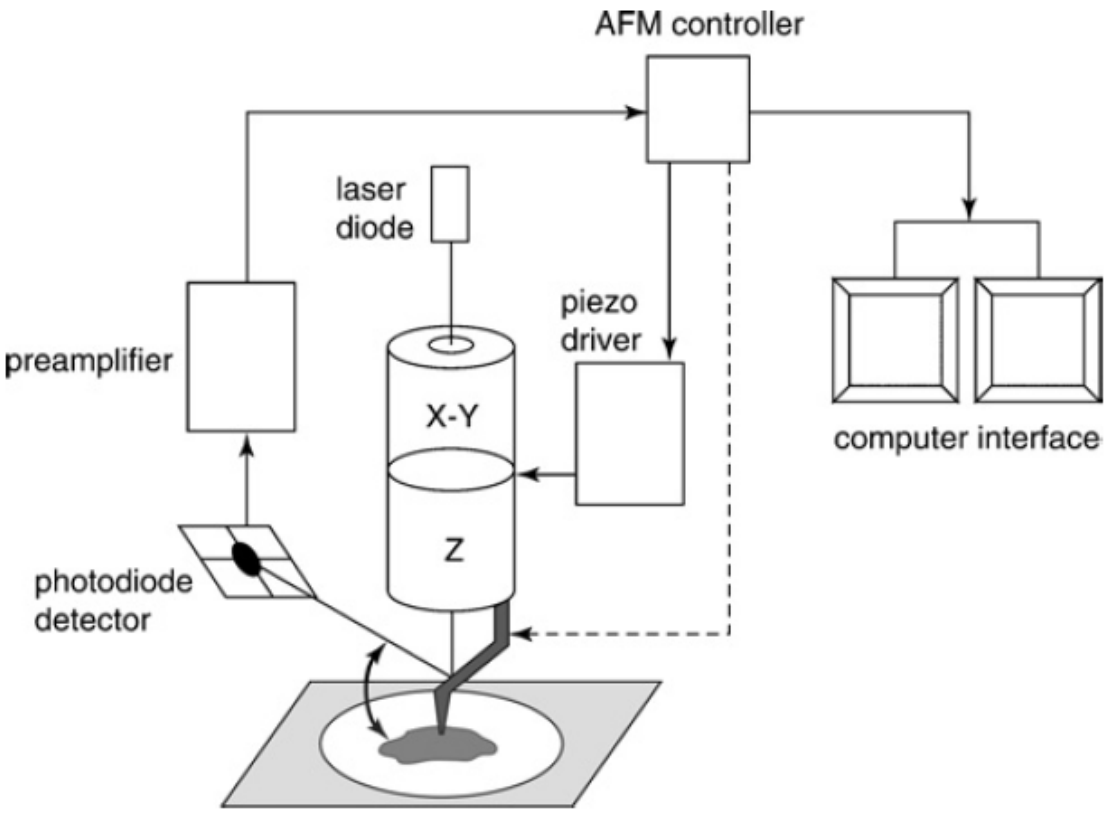

Figure II.15: Schematic illustration of the AFM system.

A laser beam coming from a laser diode is reflected off the back of the cantilever onto a photodetector. The photodetector consists of a split photodiode that senses the change in light intensity from the reflected beam due to changes in the deflection of the cantilever following tip-sample interaction.

In this way, not only the sample topography can be recorded with atomic resolution, but also material characteristics and the eventual strength of the interaction between the sample surface and the AFM tip [20] including a variety of surface roughness parameters as well as in some cases the width of surface pores and surface porosity, visualizing the effects of fouling and chemical modification on surface morphology [21].

II.3.4.2 Membrane Surface Imaging and Characterization

- **AFM Images**

  AFM images are three-dimensional scans of the surface topography, which may be obtained at a high resolution. Figure II.16 shows a 3D image of ZnO thin film elaborated using SILAR method by AFM.

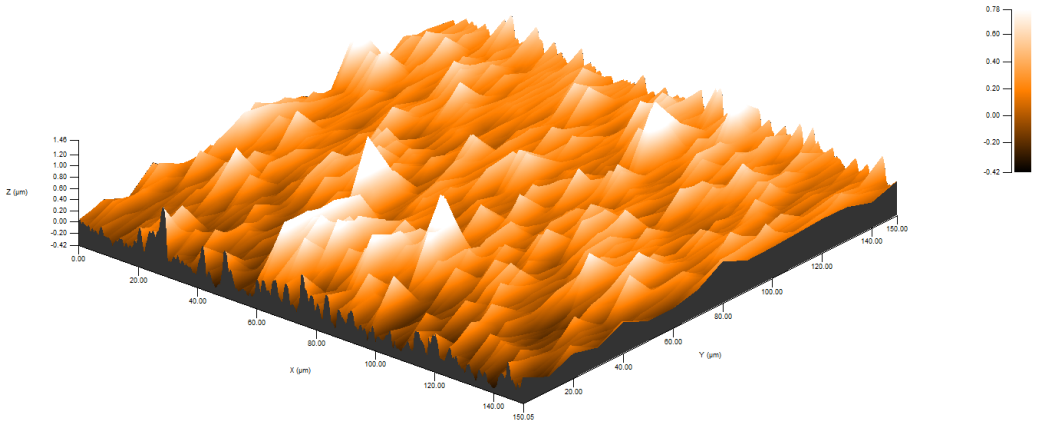

Figure II.16: AFM image.

- **Roughness Measurement**

  Most surface roughness parameters are merely a statistical measure of the variation of heights within an image or line profile taken from a surface. In the literature, the most commonly used parameters seem to be the roughness average (Ra or Sa) and the root mean squared (RMS) surface roughness (Rq or Sq).

  One important point to note is that these two measurements are affected by the size of the scan, from which the measurements are taken. For larger scan sizes, larger surface features are likely to become visible, leading to a greater height range of features included in the scan, thus increasing these statistical descriptions of height variation. This effectively means that in practice roughness values are only meaningful when comparing values obtained from scans of the same size [21].

II.3.5 Electrical Characterization

In our study, we used a four-point probe technique, by which we were able to measure sheet resistance (R_{sh}) (Resistivity and Conductivity values).

There are many developed measurement modes for conventional four-point probes as we see in Figur II.17 that can be classified into (a) a conventional collinear four-point probe for a large sample, (b) a bar-shaped thin film with four probes, (c) a conventional probing geometry for the Van Der Pauw (VDP) method, and (d) a clover-leaf vdP geometry. The most common mode is a collinear mode [22].

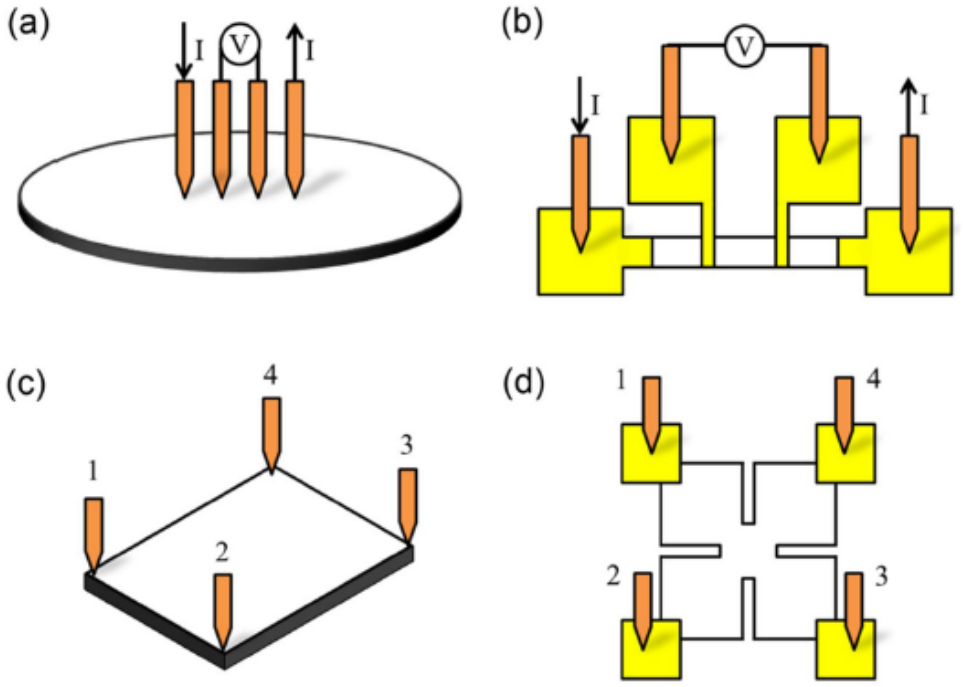

Figure II.17: Various four-probe configurations for electrical conductivity measurement of thin films.

II.3.5.1 Four-Points Probes Method

The method of the four points can be used either for a thick material or for a thin layer deposited on an insulating substrate or insulated by a junction [2].

The probe consists of four contacts aligned and regularly spaced. A source provides a current I flowing through the external terminals. The voltage U is measured across the terminals

of the two inner tips. The use of four contacts instead of two, as during a conventional resistance measurement, makes it possible to overcome the resistance of the tips and to measure only the resistance of the sample [23].

The principle of a collinear four-point probe is illustrated in Fig II.18 [24]. A current is made to flow through the outer probe pair and a voltage drop is measured across the inner pair using a voltameter with ultrahigh impedance. As a result, the measured voltage drop 'V' predominantly occurred across the semiconductor surface due to the current 'I' flowing through the sample. The four-point-probe resistance 'R' is then given by R=$\frac{V}{I}$ [25]. The use of four contacts instead of two, as during a conventional resistance measurement, makes it possible to overcome the resistance of the tips and to measure only the resistance of the sample [23].

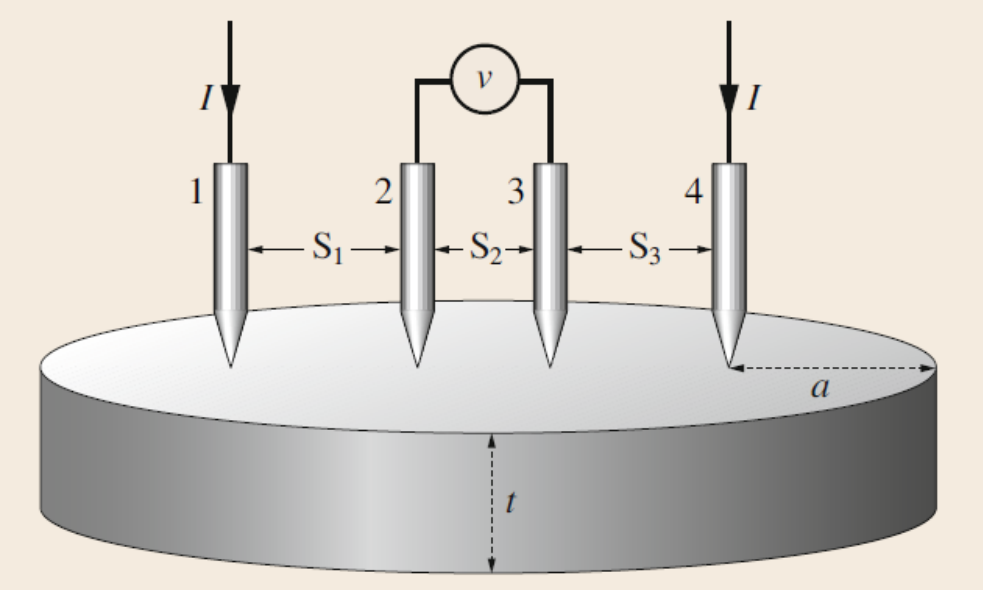

Figure II.18: Linear four-point probe configuration.

However, in order to be able to apply these formulas, 2 parameters must be taken into account with respect to the thickness (t) of the layer:

- t $\prec$ 0,1S: This makes it possible to consider that the electric field lines diffuse in the layer perpendicular to the points. In this case, it can be considered that there is no signal loss due to deep scattering in the layer.

- The tips must be located at a distance greater than 20S from the edges of the sample. This makes it possible to consider that the dimensions of the sample are infinite and

therefore avoid disturbance of the field lines generated by the limits of the sample which "reflect" the electric field [17].

II.3.5.2 Electrical Resistivity Measurement

To deduce the resistivity of the four-point measurement by knowing the thickness and the surface resistance (sheet resistance) R_{sh} is given by the relation II.14 [23]:

$$\rho = R_{sh}.t \tag{II.14}$$

Conductivity, defined as the inverse of Resistivity, is expressed by the following formula [15]:

$$\sigma = \frac{1}{\rho} \tag{II.15}$$

where:

- σ: is the conductivity $(\Omega.cm)^{-1}$.
- ρ: is the resistivity $(\Omega.cm)$.

Bibliography

[1] A BEGGAS. *Elaboration and characterization of chalcogenide thin films by chemical bath deposition technique*. PhD thesis, UNIVERSITE Mohamed Khider Biskra, 2018.

[2] S Rahmane. *ELABORATION ET CARACTERISATION DE COUCHES MINCES PAR SPRAY PYROLYSE ET PULVERISATION MAGNETRON*. PhD thesis, Université Mohamed Khider Biskra, 2008.

[3] J Bącela, M B Łabowska, J Detyna, A Zięty, and I Michalak. Functional coatings for orthodontic archwires—a review. *Materials*, 13(15):3257, 2020.

[4] DK Maurya, A Sardarinejad, and K Alameh. Recent developments in rf magnetron sputtered thin films for ph sensing applications—an overview. *Coatings*, 4(4):756–771, 2014.

[5] S P Lee. Synthesis and characterization of carbon nitride films for micro humidity sensors. *Sensors*, 8(3):1508–1518, 2008.

[6] K E Spear. Principles and applications of chemical vapor deposition (cvd). *Pure and Applied Chemistry*, 54(7):1297–1311, 1982.

[7] L Znaidi. Sol–gel-deposited zno thin films: A review. *Materials Science and Engineering: B*, 174(1-3):18–30, 2010.

[8] J Puetz and MA Aegerter. Dip coating technique. *Sol-gel technologies for glass producers and users*, pages 37–48, 2004.

[9] J Shojaeiarani, D S Bajwa, N M Stark, T M Bergholz, and A L Kraft. Spin coating method improved the performance characteristics of films obtained from poly (lactic acid) and cellulose nanocrystals. *Sustainable Materials and Technologies*, 26:e00212, 2020.

[10] N Kouidri. *Contribution à l'étude de couches minces d'oxydes transparents conducteurs à base de zinc et cobalt par spray pneumatique*. PhD thesis, University of Mohamed Khider, BISKRA, 2019.

[11] S Boulmelh. Élaboration et caractérisation d'un dépôt de couches minces d'oxyde de zinc par spray pyrolyse. *mémoire de magister, univ. Frères Mentouri Constantine*, 2015.

[12] L Filipovic, S Selberherr, G C Mutinati, E Brunet, S Steinhauer, A Köck, J Teva, J Kraft, Jö Siegert, and F Schrank. Methods of simulating thin film deposition using spray pyrolysis techniques. *Microelectronic Engineering*, 117:57–66, 2014.

[13] S Kesornkhup, A Tuantranont, T Lomas, Ch Sriprachuabwong, and K Wasapinyokul. Accuracy of swanepoel method in calculation of polymer film thicknesses. *Acta Physica Polonica, A.*, 140(2), 2021.

[14] A A Bunaciu, E G UdriŞTioiu, and H Y Aboul-Enein. X-ray diffraction: instrumentation and applications. *Critical reviews in analytical chemistry*, 45(4):289–299, 2015.

[15] A Allag. *Optimisation des conditions d'élaboration des couches minces d'oxyde d'étain SnO2 par spray*. PhD thesis, Thèse Doctorat. Université Mohamed Khider–Biskra, 2018.

[16] Sh C Navale, V Ravi, and IS Mulla. Investigations on ru doped zno: strain calculations and gas sensing study. *Sensors and Actuators B: Chemical*, 139(2):466–470, 2009.

[17] B Benrabah. *Etude des Propriétés Physico-chimiques des Couches de SnO2 Préparées par la Technique «dip-coating*. PhD thesis, Universite mohamed boudiaf'des sciences et de la technologie d'oran, 2010.

[18] S Rahmane, M S Aida, M A Djouadi, and N Barreau. Effects of thickness variation on properties of zno: Al thin films grown by rf magnetron sputtering deposition. *Superlattices and Microstructures*, 79:148–155, 2015.

[19] K Boubaker. A physical explanation to the controversial urbach tailing universality. *The European Physical Journal Plus*, 126:1–4, 2011.

[20] A Trache and G A Meininger. Atomic force microscopy (afm). *Current protocols in microbiology*, 8(1):2C–2, 2008.

[21] D Johnson, DL Oatley-Radcliffe, and N Hilal. Atomic force microscopy (afm). In *Membrane characterization*, pages 115–144. Elsevier, 2017.

[22] J Bahk, T Favaloro, and A Shakouri. Thin film thermoelectric characterization techniques. *Annual Review of Heat Transfer*, 16, 2013.

[23] J Garnier. *Elaboration de couches minces d'oxydes transparents et conducteurs par spray cvd assiste par radiation infrarouge pour applications photovoltaïques*. PhD thesis, Arts et Métiers ParisTech, 2009.

[24] M J Deen and F Pascal. Electrical characterization of semiconductor materials and devices. *Springer Handbook of Electronic and Photonic Materials*, pages 1–1, 2017.

[25] JC Li, Y Wang, and DC Ba. Characterization of semiconductor surface conductivity by using microscopic four-point probe technique. *Physics Procedia*, 32:347–355, 2012.

Chapter III

Experimental Part and Discussion

III.1 Introduction

In this chapter, we give special attention to the deposition technique of thin films by the successive ionic layer adsorption and reaction **"SILAR"**, due to the fact that it is a good alternative to the other deposition techniques because it has many advantages (which will be detailed later in addition to the general principle of SILAR), In this context that our main goal in this research task is the realization and the improvement of SILAR system to make it useful for the elaboration of thin films. Our work was carried out at The Physique of Thin Films and Their Applications Laboratory at University of Biskra.

This chapter also discusses the structural, optical, morphological, and electrical properties of a series of five samples with different cycles number (10, 20, 30, 40, 50 cycles) by using an X-ray diffractometry (XRD) device, UV-VIS spectrophotometer, atomic force microscopy (AFM), and the four-point technique respectively in order to study the effects of SILAR cycles and determine the films with optimum characteristics.

III.2 SILAR Method

III.2.1 SILAR Method Definition

The successive ionic layer adsorption and reaction (SILAR) method is a relatively new chemical deposition method for the preparation of thin films [1] and a less investigated method,

first reported in 1985 by Ristov et al. The name SILAR was ascribed to this method by Nicolau (1985) [2].

The design of the SILAR device is shown in Figure III.1, in this model 4 beakers can be used. Also, necessary set the main deposition parameters of the SILAR device such as the number of cycles(where the SILAR cycle consists of the subsequent immersion of the substrate in anionic and cationic solution and the substrate rinsing procedures in between), the immersion and immersion velocities, and the residence time at each step [3].

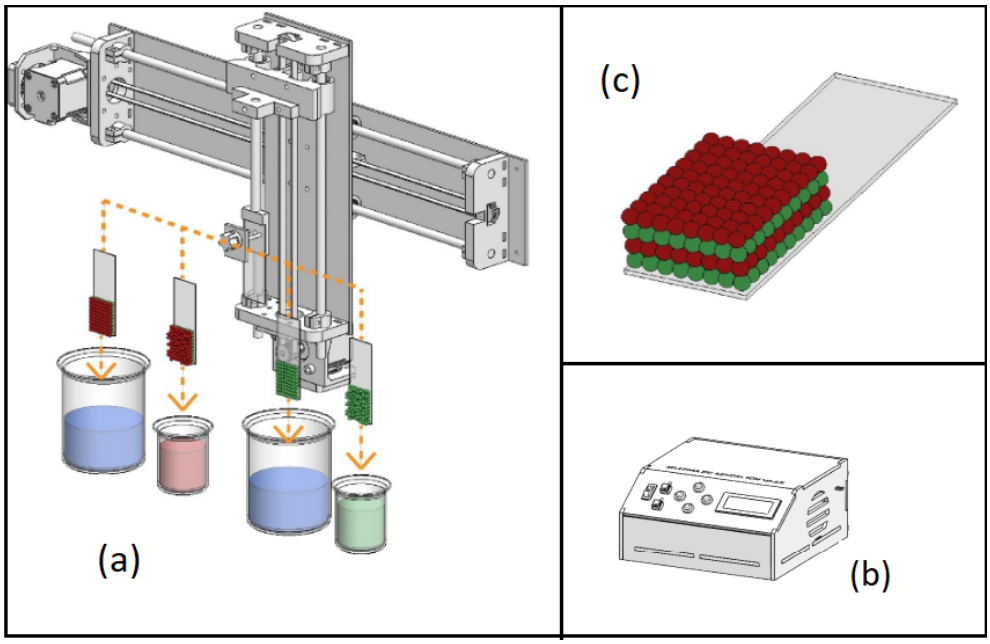

Figure III.1: Design of SILAR Device: (a) The Mechanical Structure, (b) The Control Unit, (c) Thin Film Deposition.

In the control unit, the operator needs just to clamp the substrate into the holder and program the controller with the required dip cycles and duration because It is very difficult to control dip duration and number of dips in a manual process which can last hours, also for avoid operator fatigue and errors associated with it [4]. In addition, the thickness, composition, and phase purity of thin films can be easily controlled just by regulating the growth parameters such as adsorption and reaction time, deposition cycles, and precursor concentration [5].

In figure III.2, the SILAR device which was used in this work. This device was produced by a team of academics in the laboratory of Thin films and their applications (Univ-Biskra), this system is a mechanical structure that includes a pair of rods in parallel positions that act

as a guide for a moving platform that displaces the sample in the horizontal (x) and vertical (y) axes (right and left /up and down).

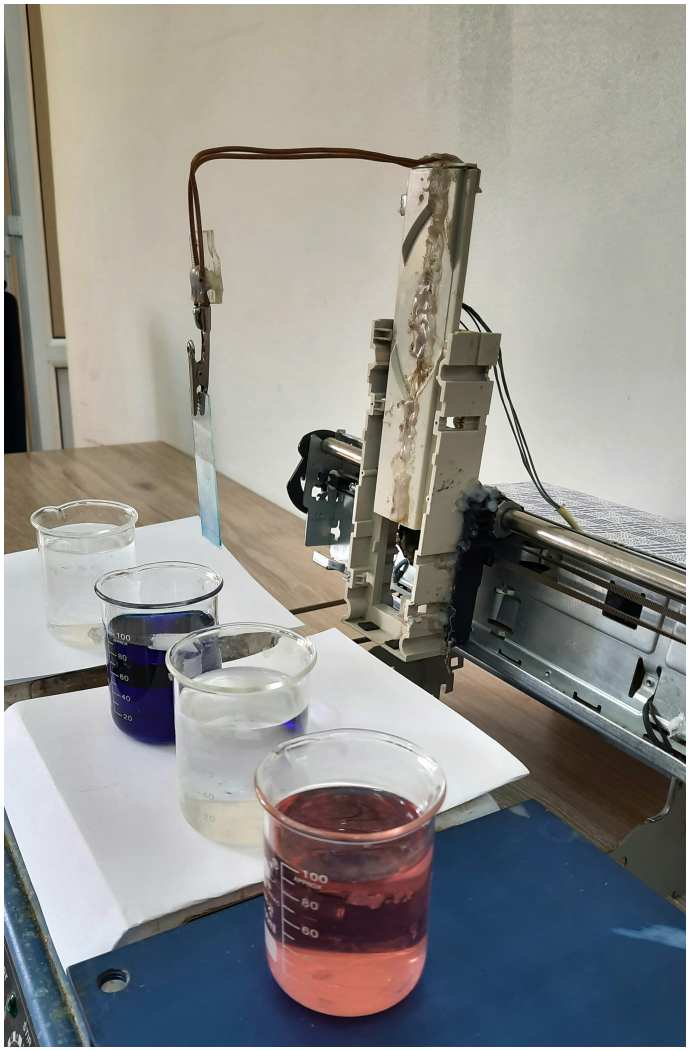

Figure III.2: SILAR device (Univ-Biskra)

III.2.2 SILAR Method Advantages

Compared with other deposition techniques, SILAR has attractive advantages such as [2, 6, 7]:

- It is a simple and economical technique that does not require highly sophisticated equipment (inexpensive).
- Unlike the closed vapor deposition method, SILAR does not require high-quality targets or substrates, or vacuum at any stage.

- The whole process is performed at room temperature and ambient pressure.
- There are virtually no restrictions on the substrate material, or dimensions, where any insoluble surface to which the solution has free access, is a suitable substrate for the deposition.
- It offers an extremely easy way to dope film with virtually any element in any proportion by merely adding it in some form of the cationic solution.

III.2.3 SILAR Method General Principle

The experimental process of SILAR involves many cycles, as shown in Figure III.3 [8] the process of one SILAR cycle where the reaction in preadsorbed cations(such as Cd^{2+}, Zn^{2+}, Fe^{3+}, Cu^{+}, etc) and newly adsorbed anions (such as SO_4^{2-}, Cl^{-}, NO^{3-}, etc) forms the thin films of the desired material, also the rinsing time in ion exchange water is critical for ionic layer formation [2]. SILAR depositions are generally conducted at room temperature, thus making them very convenient and energy efficient [9].

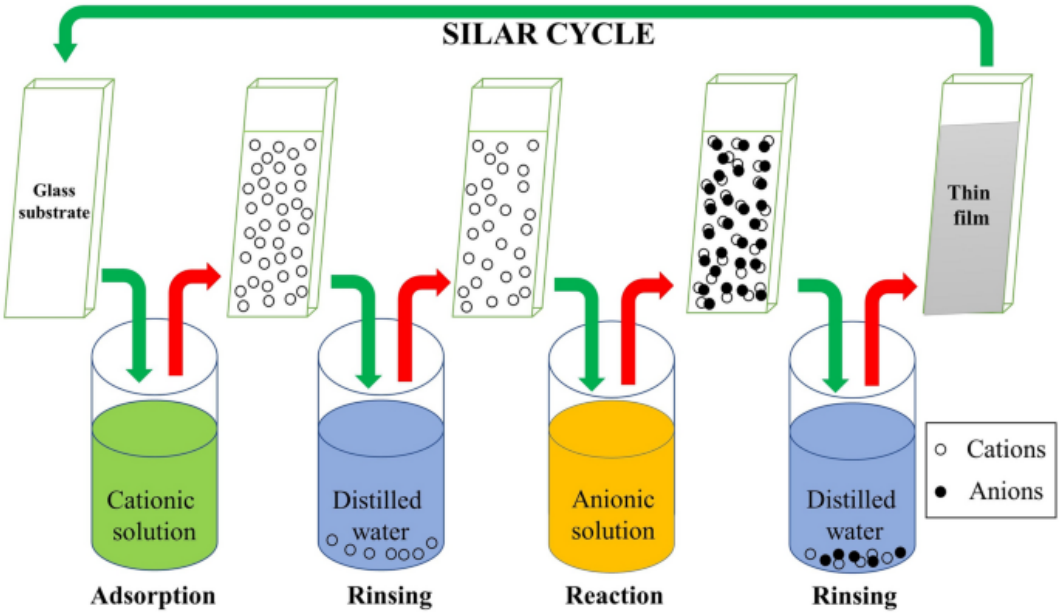

Figure III.3: Schematic representation of the SILAR technique.

The mechanism of films formation by SILAR method can be explained by discussing some equations [10] for example the ZnO films as follows [11]:

- While NH_4OH was gradually added according to the reaction, The initial white precipitate in the solution turns to a clear solution in the presence of excess ammonia by the formation of the ammonium complex ions ($[Zn(NH_3)_4]^{2+}$).

$$2ZnCl_2 + 4NH_3 \rightarrow 2[Zn(NH_3)_4]^{2+} + 2Cl^- \quad \text{(III.1)}$$

- Then, the Zn^{2+} is formed and will be adsorbed into the substrate.

$$[Zn(NH_3)_4]^{2+} + H_2O \rightarrow Zn^{2+} + NH_4^+ + OH^- \quad \text{(III.2)}$$

- Then, the substrate was immersed in the hot water in the second bath resulting in the precipitation of the $Zn(OH)_2$.

$$Zn^{2+} + 2OH^- \rightarrow Zn(OH)_2 \quad \text{(III.3)}$$

- During the heat treatment, the hydroxide phase is transformed into the oxide phase.

$$Zn(OH)_2 \rightarrow ZnO(s) + H_2O \quad \text{(III.4)}$$

When the substrate is immersed in the solution, the zinc complex ions get adsorbed surface of the substrate due to the attractive force between ions in the solution and the surface of the substrate [10], the term adsorption can be defined as the interfacial layer between two phases of a system. Adsorption may be expected when two heterogeneous phases are brought into contact with each other, it is a surface phenomenon between ions and the surface of the substrate and this is possible due to the attraction force between ions in the solution and the surface of the substrate [2]. These forces may be cohesive forces or Van-der Waals forces or chemical attractive forces [2, 10]. Atoms or molecules of the substrate surface are not surrounded by atoms or molecules of their kind on all sides, Thus, atoms can be held on the surface of the substrate [2].

III.3 Elaboration of ZnO Thin Films

III.3.1 Preparation of Substrate

The substrates used are glass slides with a square surface of 25,4 $\times$ 76,2 mm^2 and a thickness equal to 1 - 1.2 mm, this choice of glass substrates because it has many properties such as good transparency in the UV-Visible wavelength range, also, it has a thermal dilatation coefficient close to the coefficient of Zinc Oxide [12], and insulator where it will not affect the electrical measurements. All glass substrates were cleaned by:

- Washing the substrate with distilled water.
- Dipping the substrate in the dilute acetic acid (10 ml of acetic acid with 90 ml of distilled water) and then washing it with distilled water.
- Cleaning it using acetone, and after that wash it with distilled water.
- Drying using absorbant paper.

III.3.2 Deposition of Thin Film

By reading many previous studies that used the SILAR method, we noticed that the same general principle of deposition was used but with different growth procedures, and as a summary of that research, we used the following procedure which is a combination of those studies, where :

The solution for SILAR deposition was prepared by dissolving 1,363 g of Zinc chloride ($ZnCl_2$) in 100 mL distilled water (DW) with adding ammonium hydroxide solution as a complexing agent (25% NH_4OH) to form an amino complex of zinc ($[Zn(NH_3)_4]^{+2}$). This solution was stirred for 30 $\min$ at room temperature for obtaining a homogenous solution, used as a cationic solution.

In addition to an anionic solution (OH^-) consists of deionized water maintained at 80° C. First, the clean substrate was dipped in the cationic precursor to adsorb the ions of the zinc-ammonia complex and then, dipped in the anionic precursor. The adsorbed species reacted with hot water and the zinc ammonia complex transformed into zinc hydroxide [$Zn(OH)_2$], which can be transformed into a zinc oxide phase with heat treatment.

The glass substrates were coated with ZnO thin films for different numbers of SILAR cycles(10, 20, 30, 40 and 50), where the adsorption and reaction time periods are at about 20 sec. The ZnO thin films were then annealed in air at 450°C for 2 hours followed by slow cooling.

III.4 Results and Discussions

This part includes the study of different characteristics of samples prepared by changing the number of cycles from 10 to 50 like thickness, transmittance, band gap energy, crystallite size, roughness, and conductivity. In addition, discussed these experimental results and compared them with the values of other studies.

III.4.1 Thin films Thickness

In order to measure the thickness of ZnO thin films, the gravimetric method was employed using a balance with a precision of 0,1 mg. As shown in figure III.4 where thickness changes with changing the number of cycles.

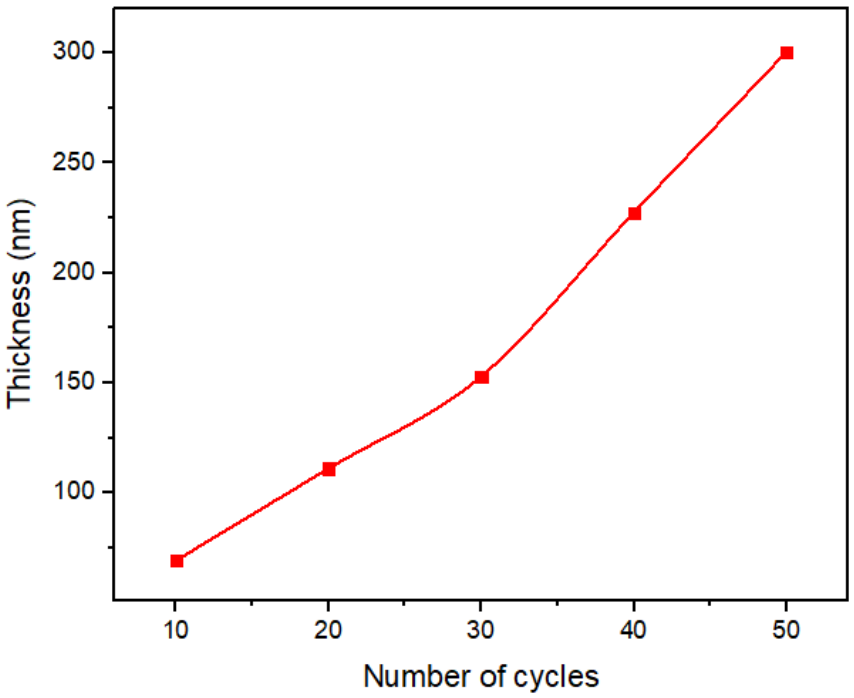

Figure III.4: Thickness variation of ZnO thin films with changing the number of cycles.

It is observed that an increase in the number of cycles resulted in an almost linear increase in film thickness, the latter is 69 , 110, 152, 227, 300 nm respectively,when the number of cycles increases from 10 to 50 cycles. this result is almost similar to the study conducted by [13] and [6], where this relationship between thickness and the number of cycles was confirmed.

III.4.2 Adhesion Test

Adhesion is a fundamental parameter in surface chemistry and physics because it depends directly on interatomic and intermolecular forces [14], where the formation and structure of the film depend on the adhesive interaction between the deposited material and the substrate [15], it also has an important role in governing the kinetics of the growth. In addition, Adhesion is very important because thin films are so fragile that they must be supported by the substrate. Where the film can share the strength of the substrate depending on the adhesion between deposited material and substrate [14].

Despite its general relevance, adhesion is one of the aspects of thin-film science about which little is known. A considerable problem arises with the measurement of adhesion, or more precisely with its lack of susceptibility to measurement [15]. initially, during the initial experiments, we confirmed thin film adhesion by rinsing a sample of the series with distilled water and then exposing it to mechanical force by rubbing it with paper. Also, before doing the characterization, all the samples were rinsed with distilled water, then after doing it, the Tape test was adopted because the peel and pull tests are capable of giving more reliable, results [16].

The results of the tape test indicate a good adhesion of the films.

III.4.3 Structural Properties

III.4.3.1 X-ray Diffraction Spectrum (XRD)

X-ray diffraction results were obtained using the device "Rigaku MiniFlex 600"(Thin films and their applications Laboratory-Biskra), using CuK_{α} radiation with a 1,541874Å-wavelength where all the samples were scanned from 25° to 50°. FigureIII.5, represents X-ray diffractograms of ZnO films as a function of cycles number.

These results indicate that ZnO films crystallized into the hexagonal wurtzite crystal structure (by comparison with JCPDS Card No.00-036-1451) with a preferential orientation along (100) plane in 31,77°.

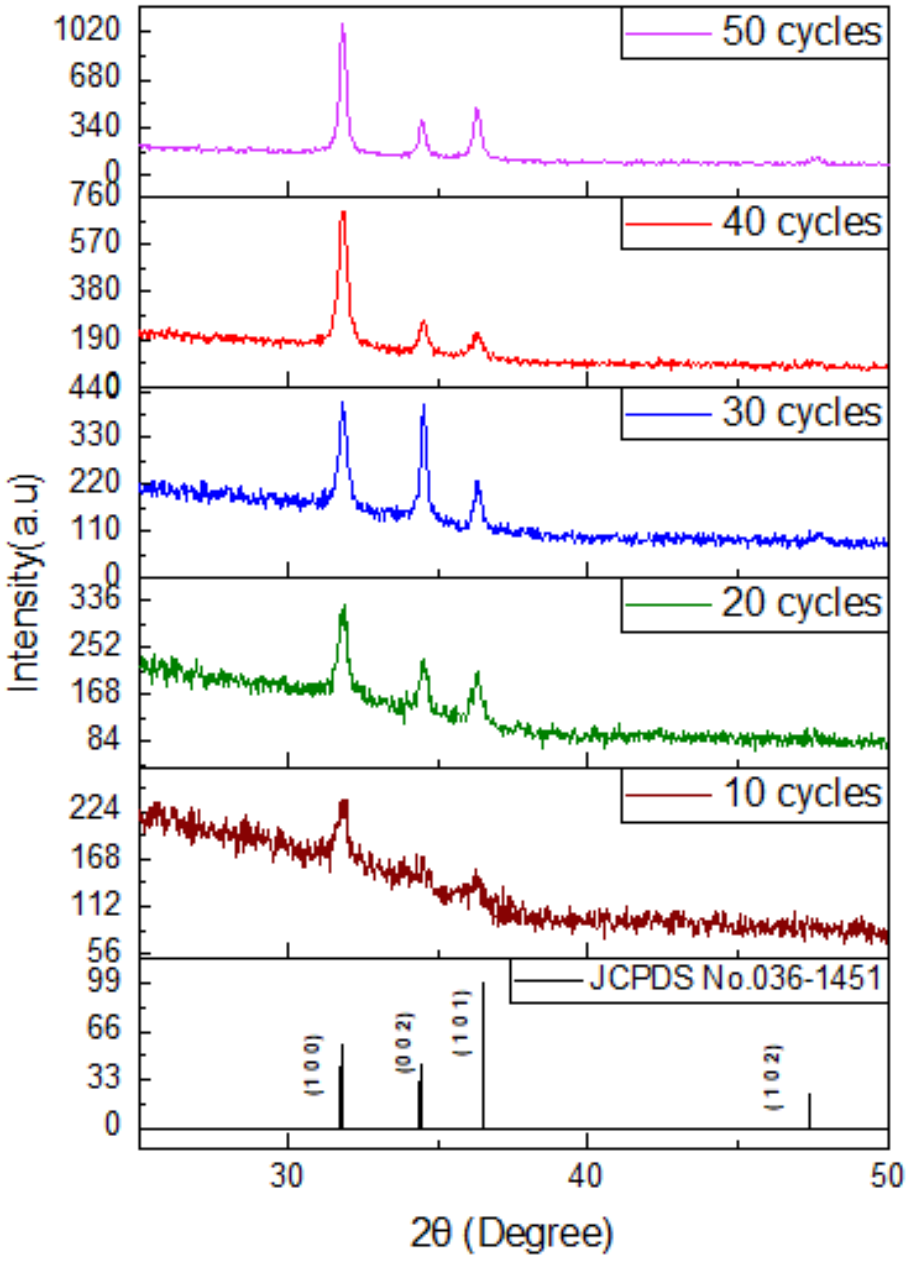

Figure III.5: X-ray Diffractogram of ZnO Films for Different Cycles Number.

This experimental result is different compared with other studies, where the (002) plane is the preferential orientation [12, 17, 18], the interpretation of these results is:

- Due to its low surface free energy [19], as stated in the report [20] that the surface free

energy of the (002) plane is not necessarily always smaller than those of other planes.

- The deposition is performed at low temperature [20–22].

Also, based on the study [23] where contained that growth conditions of these films may lead to the evolution of crystalline face energy due to imbalances of the components (Zn and O) in the area of nucleation of the crystallites, we suggest that the preference of (100) plane is due the technical conditions because films are formed due to ionic layer adsorption and reaction.

Through X-ray diffraction spectra observed starting from sample 20 cycles, the presence of secondary peaks are (002) and (101) at 34,422° and 36,253° respectively with the peak (100) which is in all samples which indicates the formation of a polycrystalline nature. Also, It is observed that an increase in the number of cycles resulted in an increase in the intensity of the peak which indicates an improvement in the crystallinity [24].

III.4.3.2 Crystallite Size and Strain

The size of the crystallites and the strain were calculated from the width at half maximum (FWHM) of the most intense (100), using Scherrer's formula. Table III.1 summarizes the corresponding values for crystallite size, strain, and lattice parameters for all the samples.

Table III.1: The values of crystallite size and strain.

Number of cycles	$2\theta_{(100)}$ (°)	$d_{(100)}$ (nm)	$d_{(002)}$ (nm)	Crystallite Size (nm)	Strain ξ	$\frac{c}{a}$
10	31,82	0,2809	/	21,4	0,603	/
20	31,88	0,2806	0,26004	30,9	0,420	1,6047
30	31,80	0,2813	0,26006	43,7	0,301	1,6009
40	31,76	0,2817	0,25975	43,7	0,302	1,5969
50	31,79	0,2814	0,26050	55,4	0,240	1,6032

To get a clear idea of this variation, we have plotted the curve of the variation of the crystallite size and strain as a function of the number of cycles as shown in figureIII.6 below.

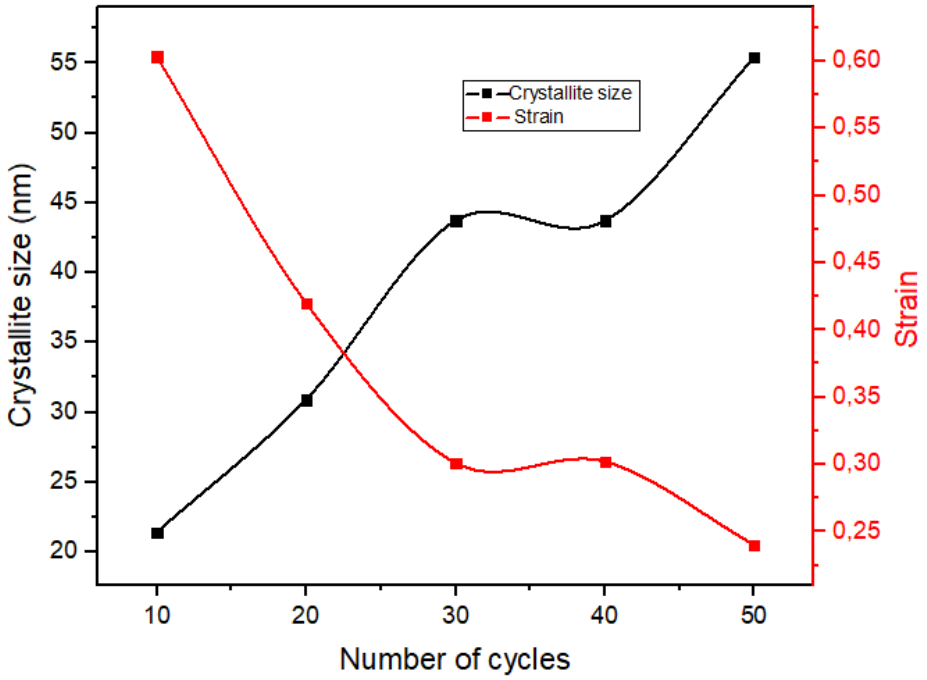

Figure III.6: Variation of Crystallite Size and Strain As a Function of Cycles Number

The graph showed the inverse relation between strain and crystallite size, while the crystallite size is increase with the number of cycles to a super-value (55,4 nm), the strain value is minimum (0,24) at 50 cycles(where the value of crystallite size is 21,4 nm and the strain value is 0,603 at 10 cycles).

The increase in the crystalline size of ZnO thin films with an increasing number of SILAR cycles was confirmed by a previous study [24], where the increase in crystallite size has been related to a rise in Crystallinity [25].

Also, the presence of strain is confirmed by $\left(\frac{c}{a}\right)$ values when compared to the theoretical value (1,6021).

Comparing the obtained values of crystallite size with other studies, we notice a convergence with the results of SILAR [24], Sol-gel [26], and Spray [27] techniques, but we can notice a big difference in of the obtained results by using the CVD method [28], where the size value was much greater.

III.4.4 Optical properties

III.4.4.1 Transmittance

JASCO V-770 UV-VIS spectrophotometer was employed in this research. In the wavelength region of 280 to 1400 nm, transmittance spectra of ZnO thin films deposited with different numbers of cycles were recorded, as shown in figure III.7.

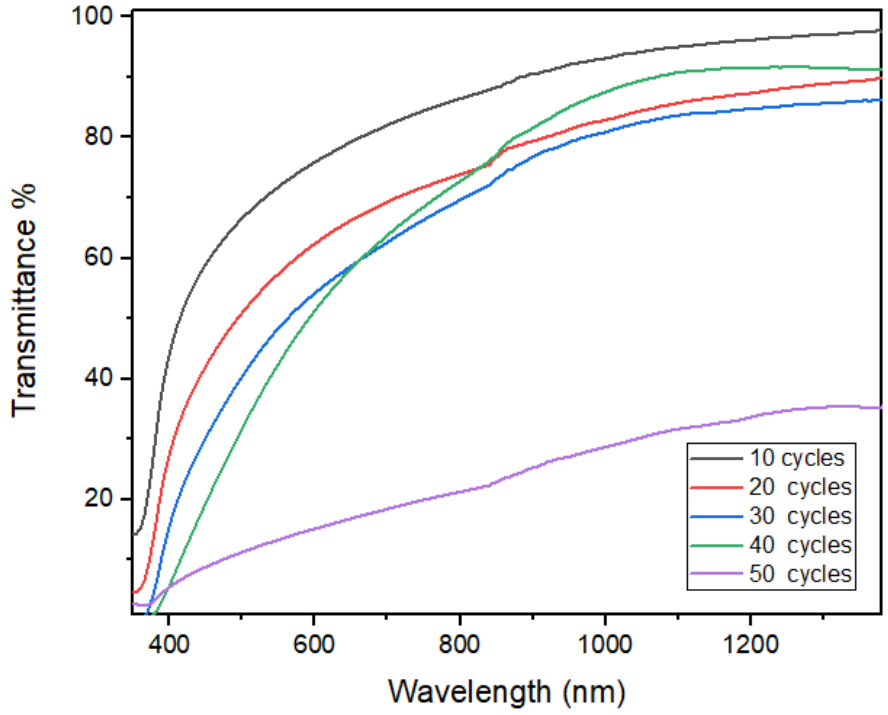

Figure III.7: Optical Transmission Spectra of ZnO Thin Films Deposited With Different Cycles Number.

From figure III.7, it is observed that the transmittance increases with the decrease in the number of cycles. We can explain this result by the increase in the thickness of the film coming from the increase in the number of cycles as shown in the Beer-Lambert equation [12, 29] which represents the inversely proportional between the optical transmission and thickness as follows [29]:

$$T = \exp^{(-\alpha.d)} \tag{III.5}$$

where T is the transmission,α is the absorption coefficient, and d is the film thickness. Also, obviously that all transmission spectra essentially contain two regions:

- A region of high transparency is located between 500 and 1300 nm, the average transmission in this range goes from 80%.
- A region between 280 and 500 nm, obviously a rapid decrease in the transparency to zero in all the samples which means a region of strong absorption.

Comparing samples results, it is evident that the sample with the fewest cycles (10 cycles) has greater transparency in which 69,096 nm is the thickness (it is the lowest thickness), this is confirmed by several other studies [13, 24].

These transmittance results are very satisfactory compared to other obtained using other deposition techniques, where it was close to the results of Spray techniques in [12] and [29], while better results were obtained by using the same technique in [13] and by using the Sol-gel technique in [30]. Also, our results are better than the transmittance results obtained by the SILAR technique in [7] and [31].

III.4.4.2 Band Gap and Urbach Energy

From the transmittance spectra, we deduced the values of the Bandgap Eg and the Urbach energy using the Tauc relationship [12, 32], the Table III.2 and figure III.8 summarize these values.

Table III.2: The values of the Bandgap Eg and the Urbach energy Eu.

Number of cycles	Bandgap Eg [eV]	Urbach energy Eu[eV]
10	3,1512	0,3658
20	3,1819	0,3711
30	3,2880	0,2177
40	3,3057	0,2246
50	/	/

The obtained values of Eg are extremely reasonable, according to a previous study on the optical band gap of zinc oxide [33]. It is observed that the optical gap (Eg) increases with the increases in the number of cycles, where it changes from 3,1512 eV (for 10 cycles)to a great value of 3,3057 eV (for 40 cycles). And we notice that the opposite happened in values of Urbach energy (Eu), where it decreases with the increases in the number of cycles from

0,3658 eV (for 10 cycles) to 0,2246 eV (for 40 cycles). It makes sense that the optical gap and disorder have an inverse relationship because, while the disorder is indicated by the breadth of the valence or conduction band tails, the optical gap is the energy difference between the band tails [34].

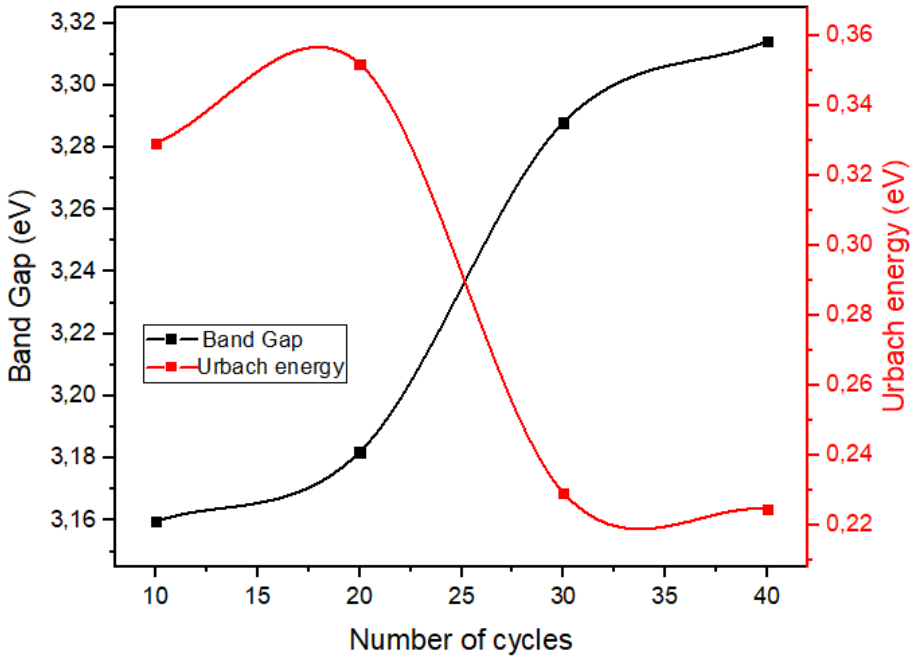

Figure III.8: The Values of the Optical Gap Eg and the Urbach Energy of ZnO Films for Different Cycles Number.

The increase in band gap can be attributed to the increases in the crystallites size, which causes the decrease in grain boundary which decreases the defects; consequently, the reduction of the disorder leads to increases in the gap [12, 34].

III.4.5 Morphological Properties

In this study, AFM analysis of ZnO thin films was conducted to get the surface morphology information by the scans of the few areas on the surface of three samples of ZnO thin films which are samples of 10, 30, and 50 cycles' samples. There surface roughness values were 0.111,0.155, and 0.192 μm respectively. Clearly, as the number of cycles increases the roughness increases, which is confirmed by the 3D photos of 150 μm × 150 μm area in Figure III.9, it also shows that the films are homogeneous.

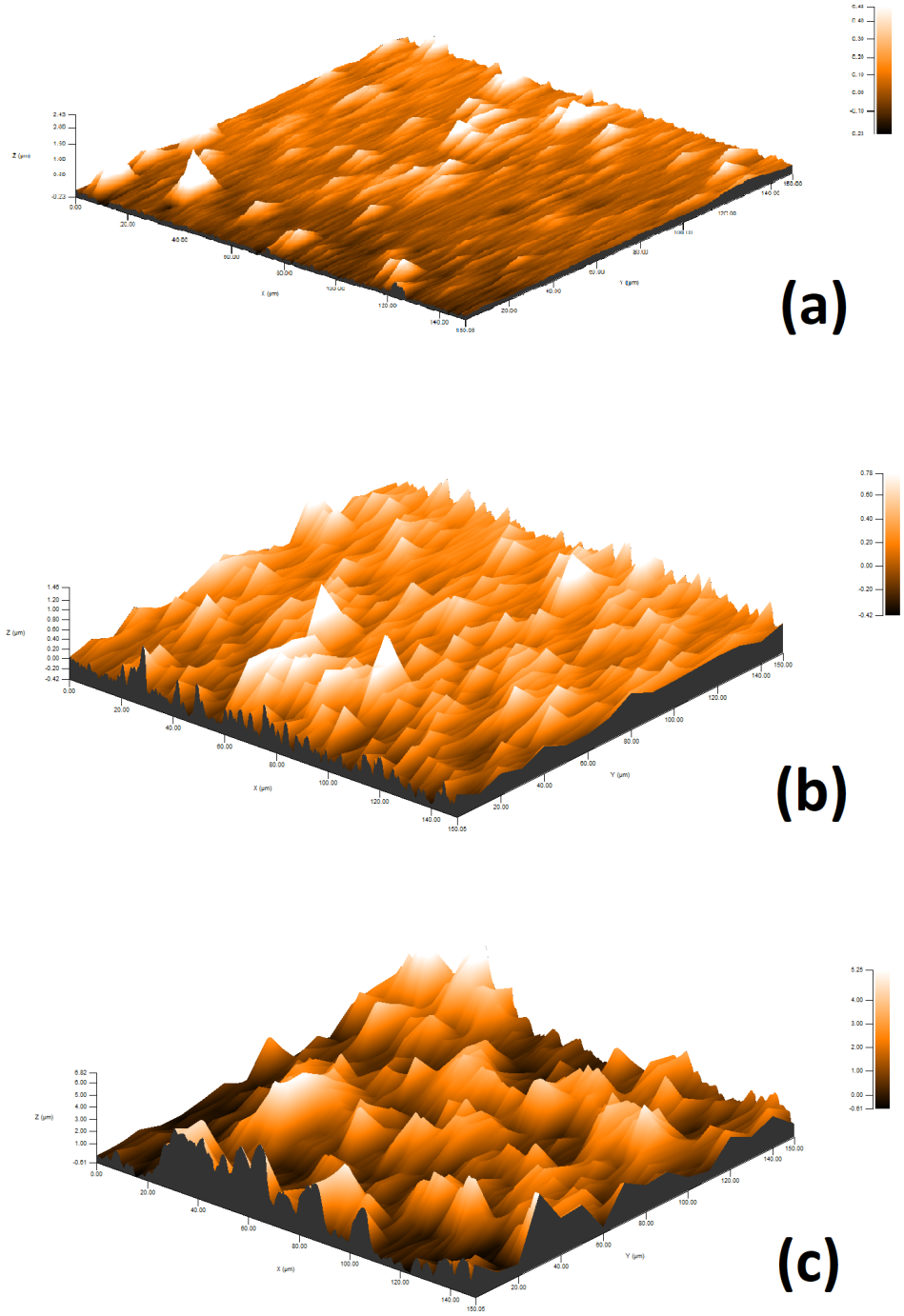

Figure III.9: AFM images (150μm$\times$ 150μm) of the ZnO films prepared under different cycles number : (a) 10 cycles ; (b) 30 cycles; (c) 50 cycles .

The growing roughness of the surfaces of these ZnO films, which is reflected by the appearance of secondary diffraction peaks [12], also the surfaces topography of the films is

indicative of the grain growth in the perpendicular direction to the substrate surface, which is in agreement with the XRD result [35]. additionally, this result confirmed what was found in the optical study where the disappearance of interference fringe in the transmittance curves of samples was a result of increasing the roughness of the surface [22].

The characterization of surface topography and roughness is imperative as the number of surface atoms and percolation path length for charge carriers to transport are dependent on surface roughness and play a dominant role in bandgap engineering [36].

III.4.6 Electrical Properties

The electrical characterization of ZnO thin films prepared with the SILAR method is carried out with the four-point probe technique using the device "KEYSIGHT B1500A"(Semiconductor Lab-univ Biskra). As a function of different cycle numbers (from 10 to 50 cycles), the measured sheet resistance, resistivity, and conductivity of ZnO thin film samples are presented in Figure III.10 and Table III.3.

Table III.3: The values of sheet resistance, resistivity, and conductivity of ZnO thin films.

Number of cycles	R sheet $\times 10^3(\Omega)$	Resistivity ρ $\times 10^{-1}(\Omega.cm)$	Conductivity σ $(\Omega.cm)^{-1}$
10	1,337	0,092	108,20
20	2,115	0,234	42,61
30	3,038	0,464	21,53
40	4,621	1,050	9,51
50	7,067	2,123	4,70

It is observed that an increase in the number of cycles resulted in an increase in film Resistivity from 0,092 to 2,123$\times 10^{-1}(\Omega.cm)$ when the number of cycles increases from 10 to 50 cycles, as is know the inverse relationship between Resistivity and Conductivity so it is logical to decrease Conductivity with the increase in the number of cycles from 108,20 to 4,70 $(\Omega.cm)^{-1}$.

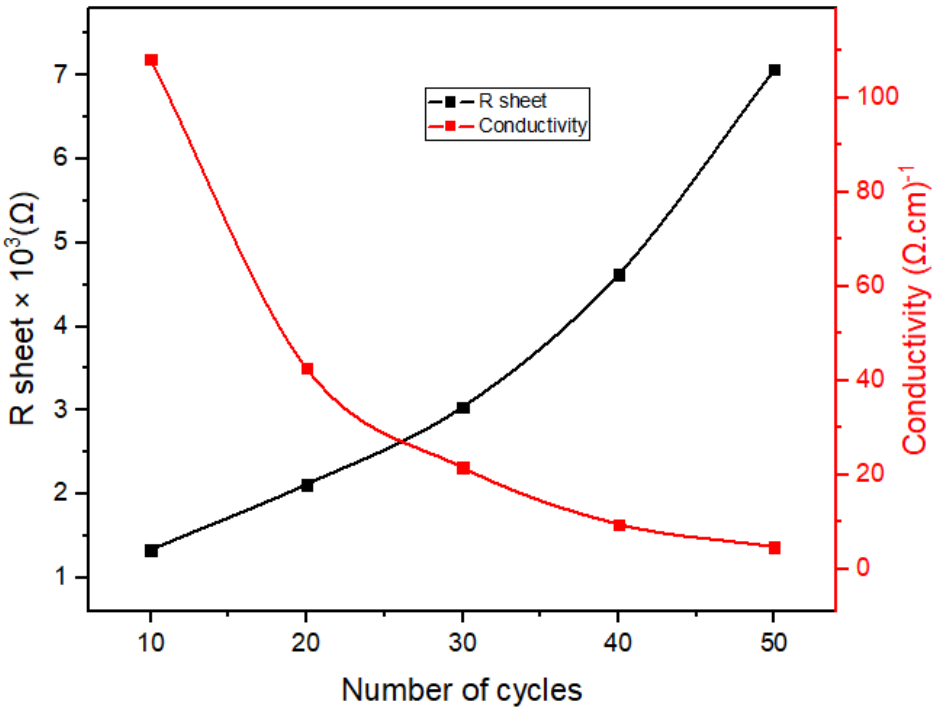

Figure III.10: The values of the sheet resistance and the conductivity of ZnO films for different cycles number.

It is customary that variations in carrier concentration and/or mobility are the cause of variations in resistivity [34].In this study, it is illogical to explain the increase in the resistivity by mobility because according to XRD spectra, the crystallite size increases (so the crystallinity of the samples improves), which leads to a decrease in the number of electrons scattering centers and trapping centers [22], so Increases in oxidation can be used to explain the decrease in conductivity, where previous studies have that with increasing SILAR cycles the presence of oxygen increases [24]. Also, using the Morphological study through the roughness values and the 3D image where the roughness of the samples increases with the increase in the number of cycles, The roughness of films leads to appear the adsorbed oxygen situated on the surface. The adsorbed oxygen captures the conduction electrons and fixes them to the surface, which leads to an increase in the electrical resistivity [22], therefore, the increase in resistivity is due to a decrease in the number of free carriers [12].

In comparison with previous studies, the results of the resistivity that we obtained were close to the results of thin films deposited using the CVD method in [28] and the SILAR method in [6], while the resistivity values in [12],[37], and [24] where these studies used

Spray, Sol-Gel, and SILAR methods respectively are high compared to our results, so we can say that the films prepared in this work have good conductivity.

III.4.7 Figure of Merit

Figure III.11 shows the quality of the films evaluated from the figure of merit Φ_{TC} expressed in Ω^{-1}, according to Haacke´s formula [38]:

$$\Phi_{TC} = \frac{T^{10}}{Rs} \tag{III.6}$$

as a function of Wavelengths from 400 to 900 nm.

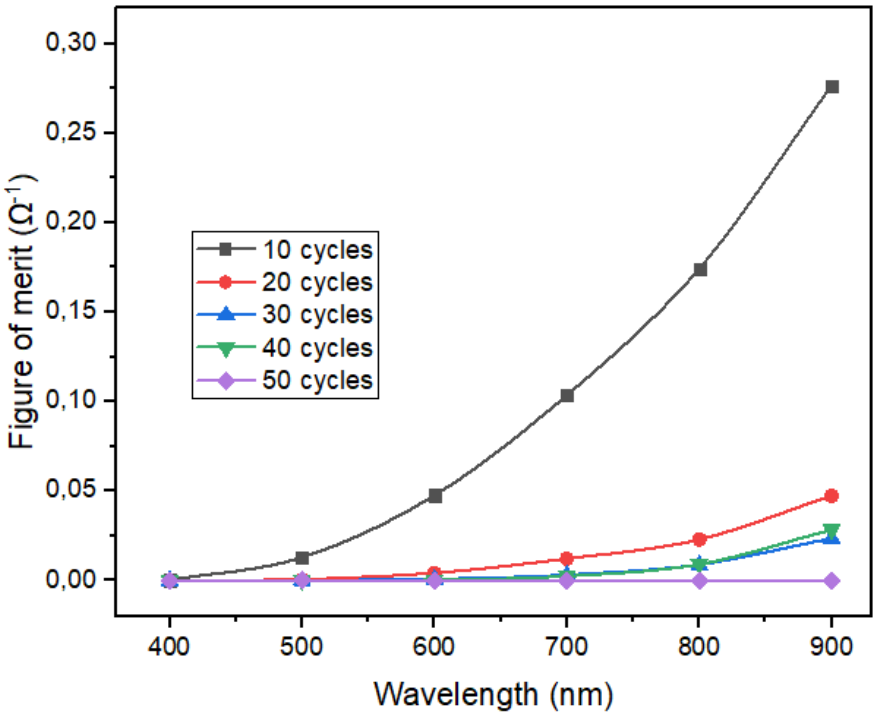

Figure III.11: Figure of merit as a function of wavelengths for different films.

It is observed that there is a decrease in the figure of merit values with the increase in the number of cycles. The figure of merit obtained of all the films is in the range of $10^{-1} \backsim 10^{-7}$ Ω^{-1}.

The sample of 10 cycles gives the higher value with Φ_{TC} = 0,0281 Ω^{-1} (at 550 nm).

In comparison with previous studies, the figure of merit results that we obtained was close to the results of ZnO thin films in [39] where prepared the zinc oxide thin films doped

with indium and aluminum by spray pyrolysis. Also, our results are better than the figure of merit ($10^{-3} \backsim 10^{-4}\ \Omega^{-1}$) for ZnO thin film in [39] and ($10^{-4}\ \Omega^{-1}$) [40] for AIZO (Al and In codoped ZnO).

Bibliography

[1] XD Gao, XM Li, and WD Yu. Synthesis and optical properties of zno nanocluster porous films deposited by modified silar method. *Applied Surface Science*, 229(1-4):275–281, 2004.

[2] HM Pathan and CD Lokhande. Deposition of metal chalcogenide thin films by successive ionic layer adsorption and reaction (silar) method. *Bulletin of Materials Science*, 27:85–111, 2004.

[3] R M Woo-García, I Rodríguez-Ibarra, E Osorio-de-la Rosa, C Guarneros-Aguilar, F Caballero-Briones, R Agustín-Serrano, A L Herrera-May, and F López-Huerta. Automated instrument for the deposition of thin films using successive ionic layer adsorption and reaction. *Processes*, 10(3):492, 2022.

[4] Holmarc Opto-Mechatronics Ltd. Silar coating system with magnetic stirrer, 2023.

[5] MA Gaikwad, MP Suryawanshi, PS Maldar, TD Dongale, and AV Moholkar. Nanostructured zinc oxide photoelectrodes by green routes m-silar and electrodeposition for dye-sensitized solar cell. *Optical Materials*, 78:325–334, 2018.

[6] G Yergaliuly, B Soltabayev, S Kalybekkyzy, Z Bakenov, and A Mentbayeva. Effect of thickness and reaction media on properties of zno thin films by silar. *Scientific reports*, 12(1):1–13, 2022.

[7] K Ravichandran, PV Rajkumar, B Sakthivel, K Swaminathan, and L Chinnappa. Role of precursor material and annealing ambience on the physical properties of silar deposited zno films. *Ceramics International*, 40(8):12375–12382, 2014.

[8] I Jellal, O Daoudi, Kh Nouneh, M Boutamart, S Briche, G Plantard, M Fahoume, and J Naja. Successive ionic layer adsorption and reaction (silar) synthesis of microstructured cu-doped zno thin films with enhanced photocatalytic activity. *Journal of Materials Science: Materials in Electronics*, 34(7):672, 2023.

[9] S P Ratnayake, J Ren, E Colusso, M Guglielmi, A Martucci, and E Della Gaspera. Silar deposition of metal oxide nanostructured films. *Small*, 17(49):2101666, 2021.

[10] H Güney and M E ERTARĞIN. Effective annealing of zno thin films grown by three different silar processes. *Eastern Anatolian Journal of Science*, 1(1):20–24, 2015.

[11] SU Offiah, SN Agbo, P Sutta, M Maaza, PE Ugwuoke, RU Osuji, and FI Ezema. Study of the extrinsic properties of zno: Al grown by silar technique. *Journal of Solid State Electrochemistry*, 21:2621–2628, 2017.

[12] S Rahmane. *ELABORATION ET CARACTERISATION DE COUCHES MINCES PAR SPRAY PYROLYSE ET PULVERISATION MAGNETRON*. PhD thesis, Université Mohamed Khider Biskra, 2008.

[13] AE Jimenez-Gonzailez and PK Nair. Photosensitive zno thin films prepared by the chemical deposition method silar. *Semiconductor science and technology*, 10(9):1277, 1995.

[14] KL Mittal. Adhesion measurement of thin films. *Electrocomponent Science and technology*, 3(1):21–42, 1976.

[15] BN Chapman. Thin-film adhesion. *Journal of Vacuum Science and Technology*, 11(1):106–113, 1974.

[16] TR Hull, JS Colligon, and AE Hill. Measurement of thin film adhesion. *Vacuum*, (3):327–330, 1987.

[17] M.A. Gaikwad, M.P. Suryawanshi, S.S. Nikam, C.H. Bhosale, J.H. Kim, and A.V. Moholkar. Influence of zn concentration and dye adsorption time on the photovoltaic performance of m-silar deposited zno-based dye-sensitized solar cells. *Journal of Photochemistry and Photobiology A: Chemistry*, 329:246–254, 2016.

[18] M Rusop, K Uma, T Soga, and T Jimbo. Optical and electrical properties of zinc oxide thin films dip-coated of sol-gel method. *Surface Review and Letters*, 12(05n06):697–701, 2005.

[19] Dae-Hyung Cho, Ji-Hong K, Byung-Moo M, Yeong-Deuk Jo, and Sang-Mo K. Control of a- and c-plane preferential orientations of zno thin films. *Applied Surface Science*, (6):3480–3484, 2009.

[20] Jianguo Lu, Zhizhen Ye, Jingyun H, Lei W, and Binghui Z. Synthesis and properties of zno films with (1 0 0) orientation by ss-cvd. *Applied Surface Science*, 207(1):295–299, 2003.

[21] C.Y. Wang, S.Y. Ma, F.M. Li, Y. Chen, X.L. Xu, T. Wang, F.C. Yang, Q. Zhao, J. Liu, X.L. Zhang, X.B. Li, X.H. Yang, and J. Zhu. The effect of mg and al co-doping on the structural and photoelectric properties of zno thin film. *Materials Science in Semiconductor Processing*, 17:27–32, 2014.

[22] Youcef Benkheta. *Elaboration and characterization of thin layers of zinc oxide (ZnO) deposited by ultrasonic spray for photovoltaic and optoelectronic applications*. PhD thesis, University Mohamed Khider of Biskra, 2019.

[23] J. Liu, S.Y. Ma, X.L. Huang, L.G. Ma, F.M. Li, F.C. Yang, Q. Zhao, and X.L. Zhang. Effects of ti-doped concentration on the microstructures and optical properties of zno thin films. *Superlattices and Microstructures*, 52(4):765–773, 2012.

[24] Vithoba L. P, Sharadrao A. V, Pramod S. P, and Jin H. K. Fabrication of nanostructured zno thin films based no2 gas sensor via silar technique. *Sensors and Actuators B: Chemical*, 239:1185–1193, 2017.

[25] F Bouaichi. *Deposition and analysis of Zinc Oxide thin films elaborated using spray pyrolysis for photovoltaic applications*. PhD thesis, University Mohamed Khider of Biskra, 2019.

[26] T. Ivanova, A. Harizanova, T. Koutzarova, and B. Vertruyen. Study of zno sol-gel films: Effect of annealing. *Materials Letters*, 64(10):1147–1149, 2010.

[27] A Allag et S Rahmane. Les proprietes structurales, optiques et electriques des couches minces de zno: Al elaborees par spray pneumatique. *Courrier du Savoir*, 20, 2016.

[28] S. Faÿ, U. Kroll, C. Bucher, E. Vallat-Sauvain, and A. Shah. Low-pressure chemical vapor deposition of zno layers for thin-film solar cells: temperature-induced morphological changes. *Solar Energy Materials and Solar Cells*, 86(3):385–397, 2005.

[29] K Nadarajah, Ch Y Chee, and Ch Y Tan. Influence of annealing on properties of spray deposited zno thin films. *J. Nanomaterials*, 2013, 2013.

[30] Z R Khan, M Sh Khan, M Zulfequar, M Sh Khan, et al. Optical and structural properties of zno thin films fabricated by sol-gel method. *Mater. Sci. Appl*, pages 340–345, 2011.

[31] P Sreedev, V Rakhesh, NS Roshima, and Balakrishnan Shankar. Preparation of zinc oxide thin films by silar method and its optical analysis. In *Journal of Physics: Conference Series*, page 012024, 2019.

[32] J Tauc and A Menth. States in the gap. *Journal of non-crystalline solids*, 8:569–585, 1972.

[33] V Srikant and D R Clarke. On the optical band gap of zinc oxide. *Journal of Applied Physics*, pages 5447–5451, 1998.

[34] A Allag. *Optimisation des conditions d'élaboration des couches minces d'oxyde d'étain SnO2 par spray*. PhD thesis, Thèse Doctorat. Université Mohamed Khider–Biskra, 2018.

[35] FN Jiménez-García, DG Espinosa-Arbeláez, C Vargas-Hernández, A Del Real, and ME Rodríguez-García. Characterization of nanostructures of zno and znmno films deposited by successive ionic layer adsorption and reaction method. *Thin Solid Films*, pages 7638–7643, 2011.

[36] A Samavati, A Awang, Z Samavati, A F Ismail, MHD Othman, M Velashjerdi, A Rostami, et al. Influence of zno nanostructure configuration on tailoring the optical bandgap: Theory and experiment. *Materials Science and Engineering: B*, 263:114811, 2021.

[37] MF Malek, N Zakaria, MZ Sahdan, MH Mamat, Z Khusaimi, and M Rusop. Electrical properties of zno thin films prepared by sol-gel technique. In *2010 International Conference on Electronic Devices, Systems and Applications*, pages 384–387. IEEE, 2010.

[38] A Allag, S Rahmane, N Kouidri, H Attouche, and A Ouahab. Polycrystalline sno 2 thin films grown at different substrate temperature by pneumatic spray. *Journal of Materials Science: Materials in Electronics*, 28:4772–4779, 2017.

[39] P Nunes, E Fortunato, and R Martins. Influence of the post-treatment on the properties of zno thin films. *Thin Solid Films*, pages 277–280, 2001.

[40] V K Jayaraman, A M Alvarez, and M De la Luz Olvera Amador. Influence of al, in codoping in enhancing the figure of merit of zno thin films for tco applications. *MRS Advances*, 2016.

General Conclusion

This study focused on elaboration and characterization of zinc oxide thin film by SILAR (successive ionic layer adsorption and reaction) technique in order to study the effect of SILAR cycles on the structural, optical, surface morphological, and electrical properties.

The structural properties of the deposited films have been analyzed using X-ray diffraction (XRD) while the optical properties are investigated by UV-VIS spectroscopy, atomic force microscopy (AFM) results allow us to characterize the morphological properties, and the electrical properties have been obtained by four probes method.

Five samples were prepared by changing the number of cycles from 10 to 50. From the results obtained during the various characterizations carried out and the corresponding discussions, it can be concluded that:

The film thickness measured by gravimetric method, found to be less than. X-ray diffraction study showes that all the films prepared in this work have polycrystalline hexagonal wurtzite phase structure with a preferential (100) orientation. Increasing the cycle number leads to increased crystallite size 21,4 to 55,4 nm, while decreasing the strain in the films.

In addition, the prepared ZnO thin films have a rough and a uniform surface with high transparency in the visible range ($\geq 80\%$) indicating the good quality of the film. The optical band gap shifts toward higher energy (from 3,15 to 3,31 eV) with the increase in cycles number, which is interpreted by the reduction of the Urbach energy from 0,37 to 0,22 eV.

Also, It is observed that an increase in the number of cycles resulted in an increase in film Resistivity from 9,2 $\times$ 10^{-3} to 2,123 $\times$ 10^{-1} $(\Omega.cm)$.

The figure of merit was in the order of 10^{-1} at 550 nm, which presents a good performance of non-doping transparent conductive oxide (TCO).

In summary, we can say that the number of SILAR cycles plays a key role in the synthesis

of ZnO thin films, which influenced the film's properties.

Finally, **the different perspectives** that can be envisaged for the rest of this work are:

- Some additional measurements could still be carried out on the ZnO films deposited during this work:
  - Hall effect resistivity measurements, this technique also mainly allows us to determine the type, density and mobility of the carriers in the films.
  - The determination of the concentration of Zinc and Oxygen atoms in ZnO films by Energy Dispersive Spectroscopy (EDS) technique.
- Ultrasonic rinsing is introduced in the SILAR method to enhance the chemical reaction.
- Finally took action and integrated the optimized ZnO layers into one of the multiple applications of ZnO.

Abstract

The present work objective is the deposition and characterization of thin films of zinc oxide (ZnO) by using successive ionic layer adsorption and reaction (SILAR) technique and discussing the structural, optical, morphological, and electrical properties of a series of five samples with a different number of cycles (for 10 to 50) in order to study the effects of SILAR cycles number and determine the films with optimum characteristics.

Where we find that film deposited at a high number of cycles (50) has the best crystallization (crystallite size about 50 nm), and a uniform surface, while the sample of 10 cycles has high transparency in the visible range (≥ 80%), with a conductivity of 108,20 $(\Omega.cm)^{-1}$ in addition to a good figure of merit (0,0281 Ω^{-1} at 550 nm).

Keywords: ZnO, Thin films, SILAR, Properties, Number of cycles.

ملخص

هدف العمل الحالي هو ترسيب وتوصيف الشرائح الرقيقة من أكسيد الزنك (ZnO) باستخدام تقنية الادمصاص والتفاعل المتتابع للطبقات الأيونية (SILAR) ومناقشة الخصائص البنيوية والضوئية والمورفولوجية والكهربائية لسلسلة من خمس عينات مع عدد مختلف من الدورات (من 10 إلى 50) من أجل دراسة تأثير عدد دورات SILAR وتحديد الشرائح ذات الخصائص المثلى.

حيث وجدنا أن الشرائح المحضرة عند عدد كبير من الدورات (50) لديها أفضل تبلور (حجم بلوري حوالي 50 نانومتر) ، وسطح موحد ، بينما العينة المحضرة عند 10 دورات تتمتع بشفافية عالية في النطاق المرئي (≤ 80٪) ، مع موصلية $108,20\ (\Omega.cm)^{-1}$ بالإضافة إلى معامل جودة جيد $0.028\Omega^{-1}$عند 550 نانومتر).

الكلمات المفتاحية: ZnO ، الشرائح الرقيقة ، SILAR ، الخصائص ، عدد الدورات.

Résumé

L’objectif du présent travail est le dépôt et la caractérisation de couches minces d’oxyde de zinc (ZnO) en utilisant une technique d’adsorption et de réaction de couches ioniques successives (SILAR) et en discutant les propriété structurels, optiques, morphologiques et électriques d’une série de cinq échantillons avec un nombre de cycles différent (de 10 à 50) afin d’étudier l’ effets du nombre de cycles SILAR et de déterminer les films aux caractéristiques optimales.

Et de là nous constatons que le film déposé à un nombre élevé de cycles (50) a la meilleure cristallisation (taille de cristallite d’environ 50 nm), et une surface uniforme, tandis que l’échantillon de 10 cycles a une transparence élevée dans le domaine visible (≥ 80%), avec une conductivité de 108,20 $(\Omega.cm)^{-1}$ en plus d’un bon facteur de mérite (0,0281 Ω^{-1} à 550 nm).

Mots clés: ZnO, Couches minces, SILAR, Propriétés, Nombre de cycles.